

EARLY SPECTRAL EVOLUTION OF CLASSICAL NOVAE:
CONSISTENT EVIDENCE FOR MULTIPLE DISTINCT OUTFLOWS

E. AYDI,¹ L. CHOMIUK,¹ L. IZZO,² E. J. HARVEY,³ J. LEAHY-MCGREGOR,¹ J. STRADER,¹ D. A. H. BUCKLEY,⁴
K. V. SOKOLOVSKY,^{1,5} A. KAWASH,¹ C. S. KOCHANNEK,⁶ J. D. LINFORD,^{7,8,9} B. D. METZGER,¹⁰ K. MUKAI,^{11,12}
M. ORIO,^{13,14} B. J. SHAPPEE,¹⁵ L. SHISHKOVSKY,¹ E. STEINBERG,^{10,16} S. J. SWIHART,¹ J. L. SOKOLOSKI,¹⁰
F. M. WALTER,¹⁷ AND P. A. WOUTD¹⁸

- ¹Center for Data Intensive and Time Domain Astronomy, Department of Physics and Astronomy, Michigan State University, East Lansing, MI 48824, USA
²DARK, Niels Bohr Institute, University of Copenhagen, Jagtvej 128, 2200 Copenhagen Ø, Denmark
³Astrophysics Research Institute, Liverpool John Moores University, Liverpool, L3 5RF, UK
⁴South African Astronomical Observatory, P.O. Box 9, 7935 Observatory, South Africa
⁵Sternberg Astronomical Institute, Moscow State University, Universitetskii pr. 13, 119992 Moscow, Russia
⁶Department of Astronomy, The Ohio State University, 140 West 18th Avenue, Columbus, OH 43210, USA
⁷Department of Physics and Astronomy, West Virginia University, P.O. Box 6315, Morgantown, WV 26506, USA
⁸Center for Gravitational Waves and Cosmology, West Virginia University, Chestnut Ridge Research Building, Morgantown, WV 26505, USA
⁹National Radio Astronomy Observatory, P.O. Box O, Socorro, NM 87801, USA
¹⁰Columbia Astrophysics Laboratory and Department of Physics, Columbia University, New York, NY 10027, USA
¹¹CRESST and X-ray Astrophysics Laboratory, NASA/GSFC, Greenbelt, MD 20771, USA
¹²Department of Physics, University of Maryland, Baltimore County, 1000 Hilltop Circle, Baltimore, MD 21250, USA
¹³INAF-Osservatorio di Padova, vicolo dell'Osservatorio 5, I-35122 Padova, Italy
¹⁴Department of Astronomy, University of Wisconsin, 475 N. Charter St., Madison, WI 53704, USA
¹⁵Institute for Astronomy, University of Hawai'i, 2680 Woodlawn Drive, Honolulu, HI 96822, USA
¹⁶Racah Institute of Physics, Hebrew University, Jerusalem 91904, Israel
¹⁷Department of Physics & Astronomy, Stony Brook University, Stony Brook, NY, 11794-3800, USA
¹⁸Department of Astronomy, University of Cape Town, Private Bag X3, Rondebosch 7701, South Africa

ABSTRACT

The physical mechanism driving mass ejection during a nova eruption is still poorly understood. Possibilities include ejection in a single ballistic event, a common envelope interaction, a continuous wind, or some combination of these processes. Here we present a study of 12 Galactic novae, for which we have pre-maximum high-resolution spectroscopy. All 12 novae show the same spectral evolution. Before optical peak, they show a slow P Cygni component. After peak a fast component quickly arises, while the slow absorption remains superimposed on top of it, implying the presence of at least two physically distinct flows. For novae with high-cadence monitoring, a third, intermediate-velocity component is also observed.

These observations are consistent with a scenario where the slow component is associated with the initial ejection of the accreted material and the fast component with a radiation-driven wind from the white dwarf. When these flows interact, the slow flow is swept up by the fast flow, producing the intermediate component. These colliding flows may produce the γ -ray emission observed in some novae. Our spectra also show that the transient heavy element absorption lines seen in some novae have the same velocity structure and evolution as the other lines in the spectrum, implying an association with the nova ejecta rather than a pre-existing circumbinary reservoir of gas or material ablated from the secondary. While this basic scenario appears to qualitatively reproduce multi-wavelength observations of classical novae, substantial theoretical and observational work is still needed to untangle the rich diversity of nova properties.

Keywords: White dwarf stars (1799), Classical novae (251), Cataclysmic variable stars (203), Spectroscopy (1558).

1. INTRODUCTION

A classical nova (CNe) is a transient event powered by a thermonuclear runaway on the surface of an accreting white dwarf in an interacting binary system (e.g., Starrfield et al. 2008, 2016). The thermonuclear runaway leads to the ejection of at least part of the accreted envelope (10^{-7} – $10^{-3} M_{\odot}$) with velocities ~ 200 – 5000 km s^{-1} and an increase in the optical brightness of the system by 8 to 15 magnitudes (Payne-Gaposchkin 1957; Gallagher & Starrfield 1978).

There is agreement that the thermonuclear runaway leads to expansion of the accreted envelope, but the mechanism(s) powering the ejection of this envelope is still highly debated and poorly understood. The energy output of the nuclear reactions may lead to the prompt ejection of part of the envelope (e.g., Starrfield et al. 2008; Shore 2014; Mason et al. 2018, 2020). The envelope will engulf the binary (for main-sequence donor stars), and the binary orbital motion energy may help eject the envelope (Livio et al. 1990; Lloyd et al. 1997). Some accreted material remains on the surface of the white dwarf, and undergoes sustained nuclear burning in a steady-state, near-Eddington luminosity phase (Wolf et al. 2013); the resultant radiation pressure can drive a wind that lasts for days to months (Kato & Hachisu 1994; Friedjung 2011). Unfortunately, there are essentially no theoretical studies that consider all of these potential mass loss mechanisms and model them self-consistently, so it remains difficult to predict which mechanism will dominate and under which conditions. Meanwhile, observations suggest that multiple mechanisms may be relevant, even within an individual system (e.g., Friedjung 1987; Strope et al. 2010; Chomiuk et al. 2014), and multiple ejections may occur over a single eruption (e.g., Pejcha 2009; Aydi et al. 2019, 2020).

Images of old nova shells show that ejecta geometries are often far from spherical. The ejecta show diverse structures including elliptical morphologies, rings, clumps, and polar caps (e.g., Shara 1995; Downes & Duerbeck 2000; O’Brien & Bode 2008). These static images imply that mass loss from novae is complex, but unfortunately these observations years-to-decades after eruption are not sufficient to reveal the physics that shaped the ejecta nor its early-time evolution. Observations obtained during the eruption itself—which can track changes in mass ejection as they occur—are needed. High-resolution optical spectroscopy during the first days of the eruption can track the velocity (and to some extent, the morphology) of the ejecta, and can therefore be used to constrain ejection scenarios in novae (e.g., McLaughlin 1945, 1947; Payne-Gaposchkin 1957;

Friedjung 1987; Williams & Mason 2010; Arai et al. 2016; Aydi et al. 2019).

1.1. *Revisiting the classics: McLaughlin, Payne-Gaposchkin, & friends*

Novae have been studied with optical spectroscopy for over a century (e.g., Clerke 1892). McLaughlin (1944) and Payne-Gaposchkin (1957) tracked the evolution of nova spectra from light-curve maximum to eventual quiescence, and noticed the appearance of multiple absorption and emission systems. These pioneering studies divided the observed systems of spectral lines into five classes based on their chronological appearance throughout the eruption, calling them the “pre-maximum”, “principal”, “diffuse-enhanced”, “Orion”, and “nebular” spectra. These historic classifications linked these systems to distinct ejecta components or shells, but did not offer extensive speculations about their origin.

Based on the classification of McLaughlin (1944), the pre-maximum spectrum appears before optical peak and is characterized by P Cygni profiles with absorption troughs at velocities of a few hundred km s^{-1} . The principal spectrum appears at or several days after optical peak, with its absorption troughs characterized by higher blueshifted velocities. The two co-exist as distinct systems for a few days before the pre-maximum system disappears. The difference in velocity between the pre-maximum and principal spectrum ranges between ~ 100 – 700 km s^{-1} and correlates with the speed class of the nova¹. According to McLaughlin (1944), once the nova has faded by \sim two magnitudes from optical peak, the diffuse-enhanced absorption system appears and is characterized by velocities around twice that of the pre-maximum components. It also shows broad emission components whose width is again correlated with the nova speed class (Payne-Gaposchkin 1957). Less than three magnitudes below optical peak, the Orion system sometimes appears, with more extreme velocities than the diffuse-enhanced spectrum and from more highly ionized species. The last distinct system of the nova eruption is the nebular spectrum, characterized by emission features of nebular and auroral forbidden lines, such as the [O III] lines and high ionization forbidden lines of iron.

Although McLaughlin (1944, 1947, 1964) and Payne-Gaposchkin (1957) provide eloquent descriptions of the evolution of the different spectral systems, the spectra themselves are not clearly illustrated in these works.

¹ Payne-Gaposchkin (1957) introduced the “speed class” classification of novae, which is based on the time it takes for the light curve to fade by two magnitudes from optical peak.

This is mainly due to the use of different tools ~ 70 years ago, which makes it difficult to compare with recent nova data sets. For example, early spectra were recorded with photographic plates, and when published, were represented in grey scale; the spectra have not reproduced well electronically (e.g., [McLaughlin 1944](#)), and are difficult to compare with modern one-dimensional spectra extracted from CCDs. Therefore, a primary aim of this paper is to revisit this pioneering work with a more modern data set, and clearly illustrate the spectral evolution of a large sample of novae near optical peak.

1.2. *Proposed explanations for multiple spectral components*

[McLaughlin \(1947\)](#) unequivocally concluded from his spectroscopic observations that there must be multiple ejecta components or shells in a given nova eruption, with the pre-maximum component external to, and expanding relatively slowly, compared to ejecta associated with the diffuse-enhanced component (see §3.1 for modern examples). He speculates that the intermediate-velocity principal component may represent material from the pre-maximum ejection, swept up and accelerated by radiation pressure from the hot white dwarf ([McLaughlin 1943](#)). While [Russell \(1936\)](#) agreed that there must be multiple ejecta components, he proposed that the principal system forms due to shock interaction rather than radiation pressure.

This scenario was revisited in a series of studies by [Friedjung \(1966a,b,c, 1987\)](#), who agreed that the light curves and spectral evolution of novae could not be explained by a single ballistic ejection, and instead conclude that multiple outflows are present. Friedjung explained [McLaughlin's](#) observations by suggesting that the principal spectrum originates from a shell that is formed by the collision of two flows—a fast wind, associated with the diffuse enhanced and Orion spectra, slamming into a slow flow, which is associated with the pre-maximum spectrum. [Friedjung \(1992, 2011\)](#) also interpreted the observed acceleration of the spectral components after optical peak in the context of a continuous radiation-driven wind from the white dwarf.

In contrast to multiple ejections, [Shore et al. \(2011, 2013, 2016\)](#) and [Mason et al. \(2018, 2020\)](#) suggested that nova ejecta are expelled in a single impulse and expand ballistically, structured as a clumpy medium with a biconical geometry. Changes in the profile of a particular line may be attributed to changes in the optical depth and ionization state of the expanding ejecta (e.g., [Shore et al. 2011](#)). [Mason et al. \(2020\)](#) studied the spectra of nova ASASSN-17hx, and argued that some spectral features are observed at the same velocities in different

species at different stages of the eruption, implying that they originate in clumps frozen in from the very start of eruption.

Recent work by [R. E. Williams et al.](#) has highlighted the possibility that not all spectral features originate in nova ejecta expelled from the white dwarf surface. [Williams et al. \(2008\)](#) pointed out the presence of absorption lines from heavy elements, such as Ti, Ba, Sc, and Y, with relatively low velocities (~ 400 to 1000 km s^{-1}). The lines are present from early on in the eruption, and last for a few days/weeks after optical peak before disappearing—they are therefore named *transient heavy element absorption* (THEA) lines. [Williams et al. \(2008\)](#) and [Williams & Mason \(2010\)](#) associated these lines with a pre-existing circumbinary reservoir of gas, perhaps from non-conservative mass transfer funneled out of the binary's outer Lagrangian points (e.g., [Taam & Spruit 2001](#); [Sytov et al. 2007](#)). However, to explain the strengths and kinematics of the THEA lines, the amount of mass and energy in this circumstellar material (CSM) would need to be uncomfortably high, rivaling the nova ejecta themselves. There is no evidence for such circumbinary reservoirs in observations of cataclysmic variables during quiescence (e.g., [Dubus et al. 2004](#); [Froning 2005](#); [Hoard et al. 2014](#)). [Williams \(2012, 2013\)](#) revised the hypothesized origin of the THEA lines to be material irradiated or ablated from the secondary star during the nova eruption. Today, the origin of the THEA lines remains a matter of debate.

1.3. *Why revisit the basics now?*

The presence of multiple spectral features and a possible link to multiple ejections and shock interaction is not limited to novae, but extends to supernovae (SNe), particularly to those showing evidence for interaction between the ejecta and a dense CSM, such as Type II_n, Type Ia-CSM, and superluminous SNe (e.g., [Chugai & Danziger 1994](#); [Chugai et al. 1995](#); [Smith et al. 2008](#); [Fox et al. 2015](#); [Dessart et al. 2016](#); [Gangopadhyay et al. 2020](#); [Jerkstrand et al. 2020](#)). Several of these studies argue that the diversity of spectral features observed in the optical and infrared spectra of SNe originate in shells created by the interaction of the SN ejecta with a complex CSM.

In addition, understanding how mass is ejected in novae has gained new urgency with the detection of GeV γ -ray emission from Galactic novae by the Large Area Telescope (LAT) on the *Fermi Gamma-Ray Space Telescope* ([Ackermann et al. 2014](#); [Cheung et al. 2016](#); [Franckowiak et al. 2018](#)). The γ -rays imply that shocks are (1) present in novae, (2) energetically important,

and (3) can dominate the optical luminosity of eruptions (Metzger et al. 2015; Li et al. 2017b; Aydi et al. 2020). The first GeV-detected nova was V407 Cyg in 2010, a system with a Mira giant secondary (Abdo et al. 2010). The white dwarf in V407 Cyg is surrounded by a dense CSM enriched by the giant wind, so it was proposed that the γ -ray producing shocks occur between the nova ejecta and this pre-existing medium (Nelson et al. 2012; Martin & Dubus 2013). However, many other *Fermi*-detected novae have dwarf companions and thus are characterized by low-density CSM. In these cases, the shocks are likely to be internal to the nova ejecta—the result of interaction between multiple colliding flows (Chomiuk et al. 2014; Metzger et al. 2015).

Radio interferometric imaging of the γ -ray detected nova V959 Mon over the first ~ 2 years of eruption showed the presence of two flows. Chomiuk et al. (2014) interpreted these two flows as an initial slow torus directed by the binary motion in the equatorial plane, followed by a fast wind which propagates more freely in the polar directions. At the interface of these two flows there are shocks that produce radio synchrotron and γ -ray emission (see Figures 2 and 3 of Chomiuk et al. 2014). Imaging of the peculiar Helium nova V445 Pup also shows a bipolar shell, equatorially confined by a dusty disk (Woudt et al. 2009), and evidence of shocks and particle acceleration in the form of luminous radio synchrotron emission (Rupen et al. 2001). Again, high-resolution radio imaging shows that the synchrotron emission originates near the dusty disk (Nyamai et al. 2020).

These multi-wavelength observations highlight the complexity and importance of mass loss in novae, and optical spectroscopy remains a critical tool for understanding it. However, only a few studies presenting modern pre-maximum spectroscopic observations of novae are available in the literature. These consist mainly of very slow novae which rise to optical peak over several weeks, and focus on explaining the peculiarities of individual novae such as HR Del (Friedjung 1992), V723 Cas (Iijima et al. 1998), V5558 Sgr (Poggiani 2008; Tanaka et al. 2011), and ASASSN-17pf (Aydi et al. 2019). Thus, for more than 70 years and since the pioneering work of McLaughlin (1944, 1947, 1964) and Payne-Gaposchkin (1957), no studies have tackled the early spectral evolution of a large sample of novae, particularly during the pre-maximum phase and early decline.

Given the ongoing debate about the mass ejection scenario in novae, we aim to solidify a unifying picture for how novae eject their accreted envelopes. In the current paper, we present pre-maximum optical spectra for a sample of 12 novae and compare them with later spec-

tra to test whether the mass-loss scenario proposed for V959 Mon can be extrapolated to other novae. Here we present a sample that uniquely combines early time coverage and high spectral resolution for a relatively large and diverse sample of novae, at least doubling the sample of novae with near-optical-peak spectra in the literature. Section 2 describes our sample and the observations. In Section 3 we present the spectroscopic results, illustrating the early spectral evolution of our nova sample, and offering more details on two particularly well-observed novae, V906 Car and FM Cir. In Sections 4 we discuss these results in the context of nova mass ejection and interaction between different flows, while in Section 5 we present our conclusions.

2. OBSERVATIONS

2.1. Sample Selection

Since novae rise to optical peak in a short period of time (from a few hours to a few days, to weeks in some extreme cases), observing novae spectroscopically before they reach optical peak is a challenging task. However, with new all-sky surveys such as the All-Sky Automated Survey for Supernovae (ASAS-SN; Shappee et al. 2014; Kochanek et al. 2017) and the advanced capabilities of citizen scientists, it is becoming more feasible to discover and report on novae before they reach their optical peak. In addition, with large telescopes capable of rapid follow-up, such as SALT, SOAR, and VLT, it is also becoming more feasible to obtain high-resolution spectra for novae near optical peak. Some citizen scientists have telescopes equipped with spectrographs, and can obtain time series of high-resolution spectroscopy for bright sources (e.g., Teysier 2019).

Therefore, we selected all recent (2013–2019) southern novae for which we obtained at least one pre-maximum spectrum (using one or more of SOAR, SALT, Magellan, or VLT). In addition we include four novae which were bright enough to be observed by citizen scientists during the rise to optical peak. Our nova sample sums up to 12 novae, all of which were observed before and after optical peak with optical spectroscopy. Each of the selected novae also had a light curve of sufficient cadence to constrain the date of the optical peak. In Table 1 we present the nova sample, listing the date of first detection in eruption (t_0) and a reference to the announcement of discovery. We also list the time of optical peak (t_{\max} ; or first optical peak in case of a nova with multiple peaks) and the V -band magnitude at optical peak (V_{\max}). Also cataloged are the time for the light curve to decline by two magnitudes from optical peak (t_2), and whether the nova was detected by *Fermi*-LAT. The quantities t_0 , t_{\max} , V_{\max} , and t_2 were derived us-

Table 1. The nova sample.

Name	t_0 (UT date)	Discovery Ref. ^a	t_{\max} (UT date)	V_{\max} (mag)	t_2 (days)	<i>Fermi</i> -detected? ^b
V1369 Cen	2013 Dec 02.7	(1)	2013 Dec 06.3	3.6	14	Y (13)
V5855 Sgr	2016 Oct 20.5	(2)	2016 Oct 24.8	7.8	13	Y (14)
V549 Vel (ASASSN-17mt)	2017 Sept 23.4	(3)	2017 Oct 17.4	9.0	100	Y (15)
ASASSN-17pf (LMCN-2017-11a)	2017 Nov 17.2	(4)	2017 Dec 07.2	11.8	121	N
FM Cir	2018 Jan 19.7	(5)	2018 Jan 28.7	6.4	150	N
V906 Car (ASASSN-18fv)	2018 Mar 16.0	(6)	2018 Mar 26.5	5.8	44	Y (16)
V435 CMa	2018 Mar 24.5	(7)	2018 Mar 29.0	10.3	60	N
V613 Sct	2018 June 29.6	(8)	2018 July 01.0	10.5	52	N
V1706 Sco (ASASSN-19mo)	2019 May 13.2	(9)	2019 May 22.0	12.3	108	N
ASASSN-19qv (SMCN-2019-07a)	2019 July 04.3	(10)	2019 July 06.4	11.2	15	N
LMCN-2019-07a	2019 July 29.1	(11)	2019 July 31.4	10.9	20	N
V1707 Sco	2019 Sept 14.1	(12)	2019 Sept 16.0	11.5	6	Y (17)

^a Discovery references: (1) = Guido et al. (2013); (2) = Nakano et al. (2016); (3) = ASAS-SN (Stanek et al. 2017); (4) = ASAS-SN (Chomiuk et al. 2018); (5) = Seach et al. (2018); (6) = ASAS-SN (Stanek et al. 2018); (7) = Nakamura et al. (2018); (8) = Sakurai et al. (2018); (9) = ASAS-SN (Stanek & Kochanek 2019); (10) = ASAS-SN (Stanek 2019); (11) = Jacques et al. (2019); (12) = Itagaki et al. (2019).

^bReferences for *Fermi*-LAT observations: (13) = Cheung et al. (2016); (14) = Nelson et al. (2019); (15) = Li et al. (2017a, 2020, in prep); (16) = Aydi et al. (2020); (17) = Li et al. (2019).

Table 2. Log of the spectroscopic observations of the novae in our sample.

Name	$t_{s1} - t_{\max}$ (days)	Instrument	R	λ Range (Å)	$t_{s2} - t_{\max}$ (days)	Instrument	R	λ Range (Å)
V1369 Cen	-1.0	ARAS	11,000	6400–6720	3.0	FEROS	59,000	3750–9000
V5855 Sgr	-1.4	ARAS	1,500	3800–7260	7.2	ARAS	1,500	3800–7260
V549 Vel	-13	SOAR-Good.	5,000	4500–5170	41.9	SOAR-Good.	1,000	4500–5170
ASASSN-17pf	-4.0	Mage-MIKE	65,000	4850–4920	3.0	Du Pont	40,000	4840–4905
FM Cir	-0.3	SALT-HRS	67,000	3900–8800	4.3	SALT-HRS	67,000	3900–8800
V906 Car	-4.4	VLT-UVES	59,000	3050–9000	1.5	VLT-UVES	59,000	3050–9000
V435 CMa	-0.2	ARAS	9,000	4000–7500	5.8	ARAS	9,000	4000–7500
V613 Sct	-0.2	ARAS	11,000	4250–7550	2.8	SALT-HRS	14,000	3900–8800
V1706 Sco	-0.0	SALT-HRS	14,000	3900–8800	7.9	SALT-HRS	14,000	3900–8800
ASASSN-19qv	-0.0	SOAR-Good.	1,000	4050–8000	3.8	SALT-HRS	14,000	3900–8800
LMCN-2019-07a	-0.0	SOAR-Good.	5,000	4500–5170	1.8	SOAR-Good.	5,000	4500–5170
V1707 Sco	-0.0	SOAR-Good.	5,000	4500–5170	1.8	SALT-HRS	14,000	3900–8800

ing data from ASAS-SN and the American Association of Variable Star Observers (AAVSO; Kafka 2020; see Section 2.3). t_2 is measured as the duration between the first peak and the last time the nova reaches two magnitudes fainter than this peak.

2.2. Spectroscopic observations

2.2.1. The spectra of the 12 nova sample

We carried out medium-resolution optical spectroscopy for several novae using the Goodman spectrograph (Clemens et al. 2004) on the 4.1 m Southern Astrophysical Research (SOAR) telescope located on

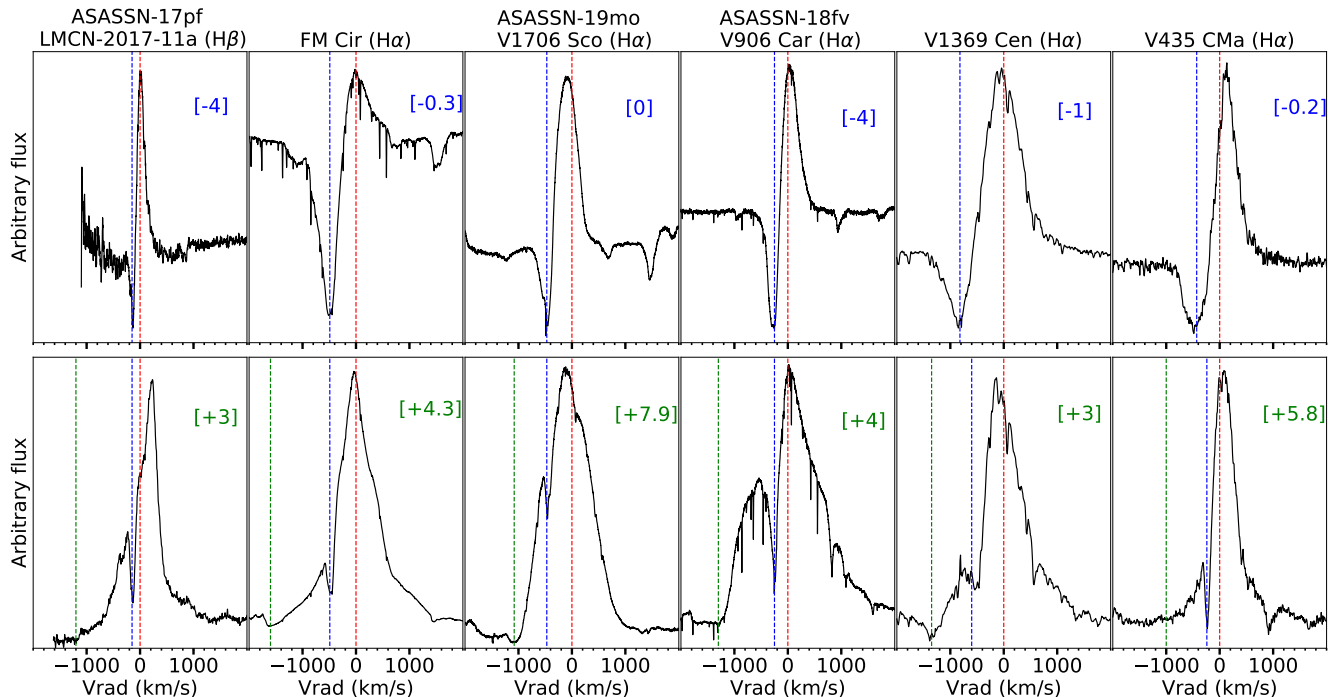


Figure 1. The line profiles of H α or H β before (*top*) and after (*bottom*) optical peak for novae LMCN-2017-11a (ASASSN-17pf), FM Cir, V1706 Sco (ASASSN-19mo), V906 Car (ASASSN-18fv), V1369 Cen, and V435 CMa. The red dashed lines represent rest velocity ($v_{\text{rad}} = 0 \text{ km s}^{-1}$). The blue and green dashed lines represent the velocities of the slow and fast components, respectively; they are centered at the minima of the absorption features or the edge of the broad emission. The numbers in brackets are the day of observation relative to the optical peak ($t_s - t_{\text{max}}$). Heliocentric correction is applied to the radial velocities in all the plots across the paper.

Cerro Pachón, Chile. Most observations used a setup with a 2100 l mm^{-1} grating and a $0.95''$ slit, yielding a resolution $R \approx 5000$ in a region centered on H α or H β that is 570 \AA wide. The spectra were reduced and optimally extracted using the APALL package in the Image Reduction and Analysis Facility (IRAF; Tody 1986). A few low-resolution spectra were obtained using the 400 l mm^{-1} grating and a $0.95''$ slit, yielding a resolution $R \approx 1000$ over the wavelength range $3820\text{--}7850 \text{ \AA}$.

We also obtained spectra using the High Resolution Spectrograph (HRS; Barnes et al. 2008; Bramall et al. 2010, 2012; Crause et al. 2014) mounted on the Southern African Large Telescope (SALT; Buckley et al. 2006; O’Donoghue et al. 2006) in Sutherland, South Africa. HRS was used in three distinct modes with a range of moderate to high resolutions, yielding $R \approx 14,000$, $40,000$, and $65,000$, over the range $4000\text{--}9000 \text{ \AA}$. The primary reduction of the HRS spectroscopy was conducted using the SALT science pipeline (Crawford et al. 2010), which includes over-scan correction, bias subtraction, and gain correction. The rest of the reduction was done using the MIDAS FEROS (Stahl et al. 1999) and

echelle (Ballester 1992) packages. The reduction procedure is described by Kniazev et al. (2016).

We obtained high-resolution spectra from the ESO/MPG 2.2m telescope with FEROS (Kaufer et al. 1999) and from the ESO-VLT 8m telescope with UVES Dekker et al. (2000). The UVES data were reduced using the reflex environment (Freudling et al. 2013) while the FEROS data were reduced using the ESO-MIDAS data analysis software (Warmels 1992).

We also make use of publicly available medium- and high-resolution spectra from the Astronomical Ring for Access to Spectroscopy (ARAS²; Teyssier 2019). For nova ASASSN-17pf, we use data from Aydi et al. (2019). These data were obtained using the Magellan Inamori Kyocera Echelle (MIKE) spectrograph mounted on the Magellan Clay telescope (Bernstein et al. 2003; Shetman & Johns 2003) and the Echelle Spectrograph mounted on the 2.5 m Irénée Du Pont Telescope³.

² http://www.astrosurf.com/aras/Aras_DataBase/Novae.htm

³ <http://www.lco.cl/telescopes-information/lco/telescopes-information/irenee-du-pont/instruments>

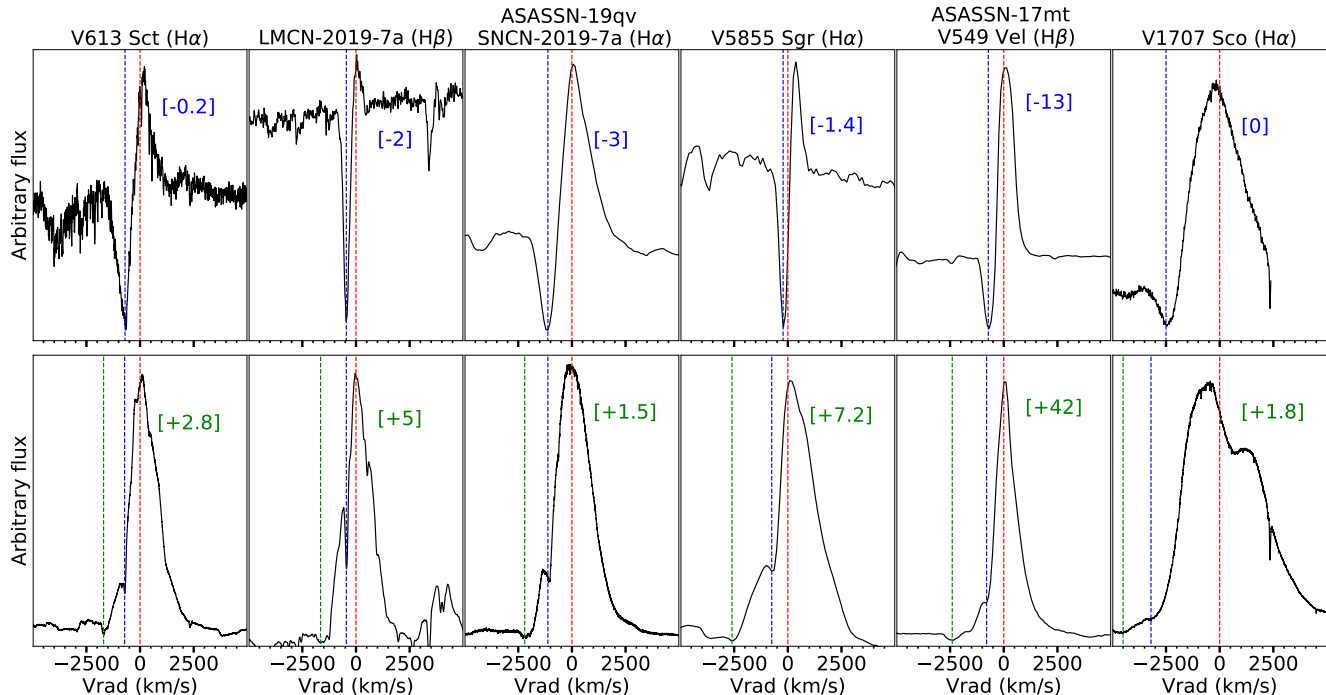


Figure 2. Same as Figure 1, but for the novae V613 Sct, LMCN-2019-7a, ASASSN-19qv (SMCN-2019-7a), V5855 Sgr, V549 Vel (ASASSN-17mt), and V1707 Sco. Note the broader velocity scale here, as compared with Figure 1; the novae plotted here show relatively fast outflows.

In Table 2 we present the details of all the spectroscopic observations, such as the times of the spectroscopic observations relative to optical peak ($t_s - t_{\max}$), the instruments used, the resolution (R) of the spectra, and their spectral ranges.

2.2.2. Additional observations of specific novae

Nova V906 Car and FM Cir were two bright, naked-eye, novae for which we have dedicated, high-resolution spectra during the rise to maximum and early decline phases. Therefore, in Sections 3.3 and 3.4 we discuss in detail the early spectral evolution of these two novae, respectively. The spectra obtained over the first 30 days of the eruption of nova V906 Car are presented in Aydi et al. 2020, and a log of these observations can be found in Table D.4 in the Appendix.

The pre-maximum spectra of nova FM Cir, during the first week of the eruption, were obtained using the CHIRON echelle spectrograph (Tokovinin et al. 2013) mounted on the CTIO 1.5m telescope. All observations were made in queue mode by professional observers. Integration times were typically 10 minutes in a single integration, but multiple integrations were obtained and summed on some nights. Spectra were taken in both “fiber mode”, with 4×4 on-chip binning yielding a resolution $R \approx 27,800$, and with the image slicer (“slicer

Table 3. Log of the spectroscopic observations of the very fast novae V659 Sct (ASASSN-19aad) and V407 Lup (ASASSN-16kt).

Name	$t_{s2} - t_{\max}$	Instrument	R
(days)			
V659 Sct	5.3	SOAR-Goodman	5,000
V407 Lup	5.0	VLT-UVES	59,000

mode”), with 3×1 on-chip binning yielding a resolution $R \approx 78,000$ over the range of 4100–8900 Å. A log of these observations is presented in Table D.5.

2.2.3. Sample bias and very fast novae

Our sample is biased towards slower evolving novae, since faster novae rise to maximum in $\lesssim 1$ day and therefore are more challenging to observe before peak. We have obtained post-maximum spectra of two very fast novae (V407 Lup and V659 Sct). We did not have pre-maximum spectra for these objects, so they are not included in our main sample. Still, these post-maximum spectra, obtained using VLT-UVES and SOAR during the early decline, are useful for extending conclusions about spectral evolution to the fastest-evolving ejections. The log of these observations is listed in Table 3.

2.3. Light curves

We construct an optical light curve for each nova using V -, and/or g -band data from ASAS-SN and the AAVSO. For some novae, we augment V and g light curves with visual and CV (unfiltered observations with V magnitude zero-point). We present the light curves for all the novae in the sample in Appendix A. These light curves are plotted around optical peak to highlight the early evolution and show the dates of the spectroscopic observations on the plot. The peak is measured from the V or g -band light curves as the date when the light curve reached its highest brightness. For novae with multiple peaks/flares, we consider the peak as the date when the light curve reaches its first peak.

3. RESULTS AND ANALYSIS

In this section, we first present the early spectral evolution of the Balmer lines for all the novae in our sample. Then we present a more detailed view on the spectral evolution of novae V906 Car and FM Cir, considering lines beyond the H Balmer series and including THEA lines during the rise to peak and early decline. At the end we highlight some general trends that we noticed in these two novae and other well-observed novae in our sample.

3.1. Consistent evidence for two flows in all the novae of our sample

In Figures 1 and 2 we present the $H\alpha$ or $H\beta$ line profiles, shortly before and after optical peak, for each nova in our sample. The novae are grouped in increasing order of the full width at zero intensity (FWZI) of the post-peak emission lines, for a better illustration. The reason we choose to highlight the evolution of the Balmer lines for all novae is that several of our medium- and high-resolution spectra cover limited spectral ranges centered on $H\alpha$ or $H\beta$. Additional lines are studied for some well-observed novae in our sample and will be discussed in following sections.

All the novae show a similar spectral evolution: before optical peak, the emission lines show P Cygni profiles with absorption troughs at velocities ranging between -200 and -1000 km s^{-1} , correlated to the speed class of the nova. Shortly after optical peak, a broad emission component emerges with the base of the emission extending to velocities $>1000 \text{ km s}^{-1}$ (more than twice the velocity of the pre-maximum component), while the pre-existing P Cygni profiles are superimposed on top of the broad emission line profiles. The broad emission is sometimes accompanied by a blue-shifted absorption feature that is relatively weak compared to the emission. For some of the fast novae in our sample, such as

V1707 Sco (Figure 2), the narrow component is difficult to see after optical peak without a zoom-in on the absorption of the P Cygni profile. This is mainly due to the nova being very fast and thus the absorption feature weakening rapidly.

Hereafter we call the pre-maximum P Cygni profile the “slow component” and the post-maximum broad emission + higher-velocity P Cygni absorption the “fast component”. These are probably the same as the “pre-maximum” and “diffuse enhanced” systems of McLaughlin (1944), though quantitative comparison between modern one-dimensional spectra extracted from CCD images and reproduced older two-dimensional photographic plate spectra is challenging.

The co-existence of the slow and fast components indicates the presence of at least two physically distinct flows, a slow and a fast one. The superimposition of the slow P Cygni profile on top of the broad emission indicates that a significant portion of the fast flow is inside the slow flow. We return to these points in Section 4.1.

3.2. Very fast novae

The light curves of very fast novae reach optical peak in roughly a day, which makes it challenging to obtain spectroscopic observations before peak brightness (Warner 2008). For the fast novae in our sample, which we manage to observe before or at optical peak (V1707 Sco and ASASSN-19qv in Figure 2), we observe the same spectral evolution as seen in slower novae.

For other very fast novae, observations before optical peak were not feasible, but the post-maximum spectra still show evidence of the slow and fast components. In Figure 3 we present two additional examples of very fast novae, V407 Lup (ASASSN-16kt) and V659 Sct (ASASSN-19aad). These novae have $t_2 \approx 3$ days (Aydi et al. 2018) and 6 days (based on AAVSO data), respectively. The $H\alpha$ line profiles of both novae show a slower P Cygni profile superimposed on top of a broader emission base. This is additional evidence that the two-flows scenario is common to all novae, regardless of their speed class.

3.3. The spectral evolution of nova V906 Car

Nova V906 Car (ASASSN-18fv) was discovered in eruption in March 2018 by ASAS-SN (Stanek et al. 2018) and peaked at ~ 5 mag in the optical. The nova was observed extensively from radio to γ -ray and has already been the topic of multiple studies (Molaro et al. 2020; McLoughlin et al. 2020; Aydi et al. 2020; Pavana et al. 2020; Wee et al. 2020; Sokolovsky et al. 2020). Aydi et al. (2020) detected a correlation between flares in its optical and γ -ray light curves, which led them

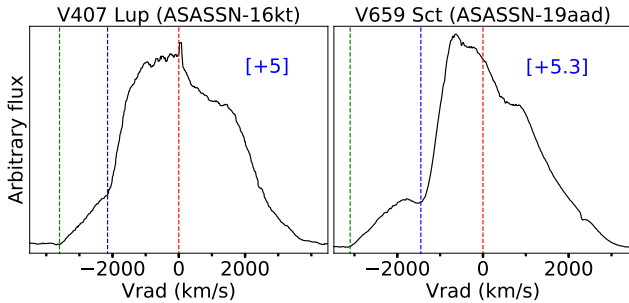


Figure 3. The $H\alpha$ line profiles of the very fast novae V407 Lup (*left*) and V659 Sct (*right*), taken around 5 days after their respective optical peaks. Despite the very rapidly evolving light curves of these novae, we still observe the slow (blue dashed line) and fast (green-dashed line) components co-existing in their line profiles. The red-dashed line represents $v_{\text{rad}} = 0 \text{ km s}^{-1}$.

to conclude that shocks are the source of a substantial fraction of the nova optical luminosity (in contrast to the standard picture of a nuclear-burning white dwarf powering the bolometric luminosity). High resolution optical spectra were obtained for this moderately fast nova during the rise and early decline, with a cadence of around 1 day, making it an ideal case to study the spectral evolution of novae near optical peak.

Figure 4 shows two full spectra of V906 Car, obtained before and after optical peak. In addition to the typical nova emission lines of H I, Fe II, and O I, the spectra are characterized by large numbers of absorption features, which we associate with THEA lines and which we discuss in § 3.3.4. These lines appear less prominent in the post-maximum spectrum because at this stage the emission lines become very strong.

3.3.1. The Balmer lines

In Figures 5 and 6, we plot the line profile evolution of $H\alpha$ and $H\beta$ for V906 Car. During the rise to maximum, the lines show P Cygni profiles with absorption troughs centered at blueshifted velocities of $\sim 200\text{--}250 \text{ km s}^{-1}$ (the slow component). The emission components of the P Cygni profiles fade relative to the continuum during the rise to maximum, as the equivalent width (EW) of the emission components weakens from $\text{EW} = -5 \text{ \AA}$ on day -4 to $\text{EW} = -0.3 \text{ \AA}$ around peak.

Around a day after peak, a broad emission line component emerges with the P Cygni profile superimposed on top of it. The broad emission is accompanied by a broad and relatively shallow P Cygni absorption component at $\sim -1200 \text{ km s}^{-1}$ (the fast component). Note how suddenly this fast component appears, between day 0 and 1. The fast emission line component gradually broad-

ens after optical peak and its P Cygni absorption moves blueward. After the light curve peaks, the pre-maximum P Cygni profile changes gradually into a double peaked emission profile, which becomes prominent around 10 days after optical peak.

3.3.2. The Fe II (42) and O I lines

The other prominent lines in the spectrum such as the Fe II (42) multiplet and O I lines show the same spectral evolution as the Balmer lines (Figure 7). They start with pre-maximum slow P Cygni profiles, and later develop another broader P Cygni component, while the original slow absorption remains superimposed on the fast component, showing that this evolution is consistent across the different prominent lines.

3.3.3. The intermediate component

A closer look at the low velocities of the prominent lines shows that at optical peak a new distinct component appears at a velocity of around -300 km s^{-1} , co-existing with the slower pre-maximum component at -200 km s^{-1} (see Figure 8 where we plot the Na I D, H I, Fe II, and O I lines, focusing on the lower velocities). This intermediate velocity system is what McLaughlin calls the “principal system” (McLaughlin 1944; Payne-Gaposchkin 1957) and we call it the “intermediate component”, hereafter. While initially blended with the slower pre-maximum component, a few days after peak the intermediate component starts replacing the slower, pre-maximum component. Moreover, both components move blueward, showing a gradual acceleration after peak. In Section 4 we interpret the origin of the intermediate component.

For the Na I D line the slow component disappears after a couple of days from peak, while for the Balmer lines the slow component lasts a bit longer and stays dominant till around 4 days after peak, when the intermediate component starts replacing it. This means that comparing the Balmer line evolution near optical peak for other novae and assuming that the same slow component is still superimposed on the fast component a few days after optical peak is reasonable.

3.3.4. The THEA lines

The spectra of nova V906 Car show a large number of THEA lines present from the first epoch obtained 4 days before optical peak (see Figure 4). We show some of the THEA lines in comparison with the Na I D2 line at 5889.9 \AA in Figure 9. More THEA lines are plotted in Figures B.1–B.4.

Four days before peak, the lines show an absorption feature at around -200 km s^{-1} (consistent with the slow component seen in other lines). Around optical peak a

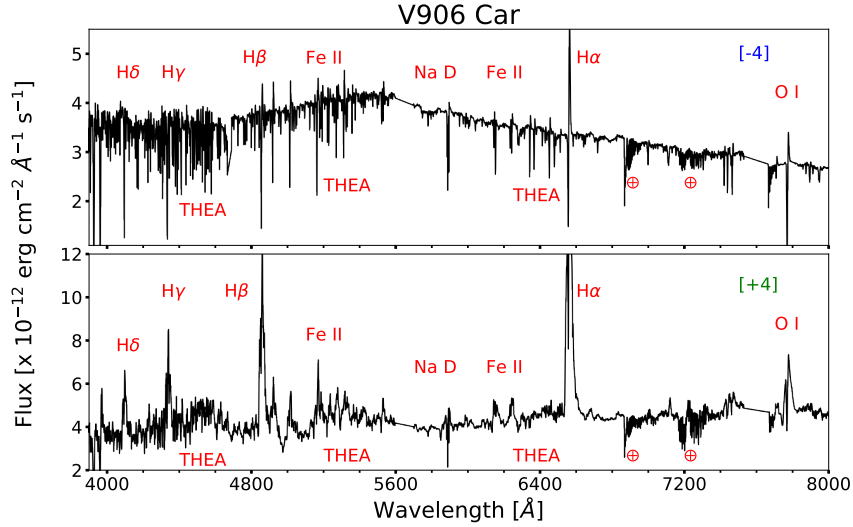


Figure 4. UVES high-resolution spectra of **nova V906 Car**. The numbers in brackets are days relative to optical peak. Prominent lines are labelled, and telluric features are marked with an Earth symbol.

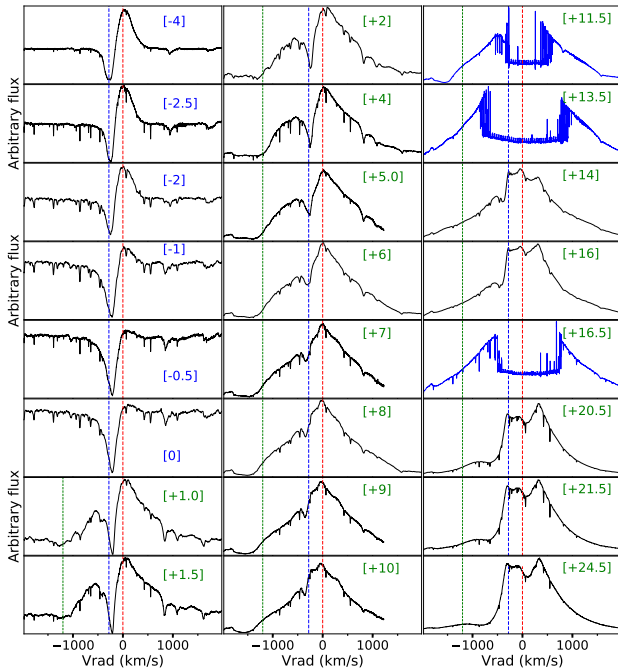


Figure 5. The evolution of the $H\alpha$ line profile of **nova V906 Car**. The numbers in brackets are days relative to optical peak. The red vertical dashed line represents $v_{\text{rad}} = 0 \text{ km s}^{-1}$ (rest wavelength). The blue vertical dashed line marks a velocity of -250 km s^{-1} to highlight the velocity variation of the slow component. The green dashed line marks a velocity of -1200 km s^{-1} to highlight the velocity variation of the fast component. The profiles shown in blue with a centred “notch” are saturated and are shown to illustrate the changing width of the fast component (see Aydi et al. 2020).

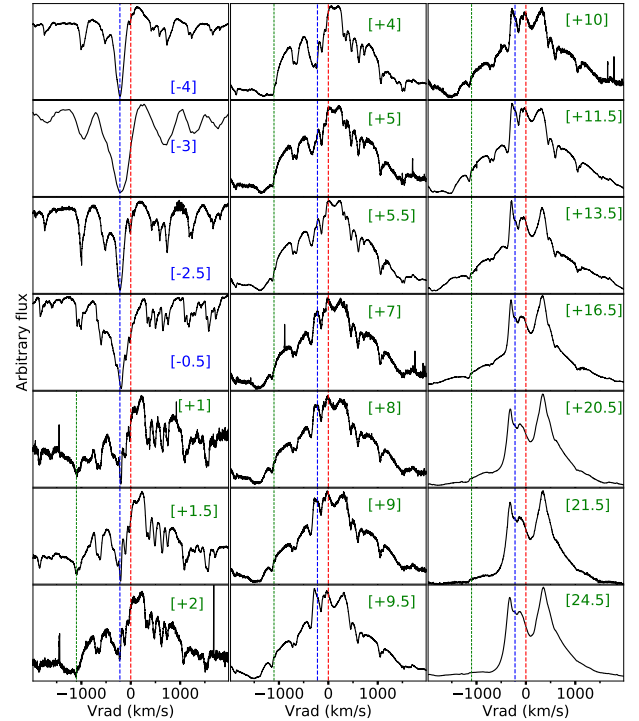


Figure 6. The evolution of the $H\beta$ line profile of **nova V906 Car**. The red vertical dashed line represents $v_{\text{rad}} = 0 \text{ km s}^{-1}$ (rest wavelength). The blue vertical dashed line marks a velocity of -200 km s^{-1} to highlight the velocity variation of the slow component. The green dashed line marks a velocity of -1100 km s^{-1} to highlight the velocity variation of the fast component. The numbers in brackets are days relative to optical peak.

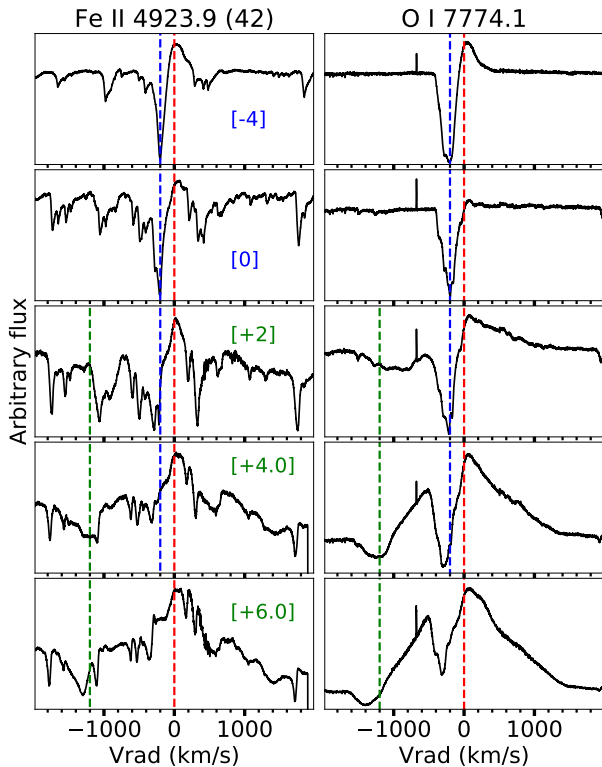


Figure 7. The line profile evolution of one of the Fe II (42) and O I lines for *nova* V906 Car. The red vertical dashed line represents $v_{\text{rad}} = 0 \text{ km s}^{-1}$ (rest wavelength). The blue vertical dashed line marks a velocity of -200 km s^{-1} highlighting the slow component. The black dashed line marks a velocity of -1200 km s^{-1} highlighting the fast component.

new system appears at a velocity of around -300 km s^{-1} , co-existing with the slower feature (the intermediate component). A couple of days after peak, the intermediate component replaces the slower, pre-maximum system and shows a gradual acceleration.

Unlike the Na I D, H I, Fe II, and O I lines, we do not detect the “fast component” of $\sim -1200 \text{ km s}^{-1}$ in the THEA lines. In Figure B.5 we show some THEA line profiles plotted with an extended velocity scale, to -1500 km s^{-1} to show the absence of a fast component. It is possible that the THEA lines do not develop a fast component, or that the fast component in the THEA lines is too weak to be detected. We compare the EW of the pre-maximum components of the Fe II (42) lines with the EW of the same components in THEA lines. The THEA EW are $0.1\text{--}0.6\times$ the EW of the Fe II lines. Therefore, if the line ratio between the slow and fast components in a specific transition is the same for all transitions (e.g., the EW ratio between the slow and fast components of Fe II 5018 is equal to that of the THEA

lines), we should expect to detect the fast component in some THEA lines, particularly the stronger ones. However, the optical depth of some transitions of Fe II (42) is larger than for the THEA lines and therefore might affect this ratio. Also, the difference in densities and possibly abundances between the fast and slow flows might be another reason for why we do not observe a fast component in certain transitions, particularly the THEA lines.

Except for the fast component, the THEA lines show the same evolution as the Na I D, Fe II (42), and O I lines (Figure 8). That is, they develop the same slow and intermediate components at approximately the same velocities at approximately the same time.

3.4. The pre-maximum spectral evolution of THEA lines in *nova* FM Cir

Nova FM Cir was another bright nova (peaking at ~ 5 mag), discovered in January 2019 by (Seach et al. 2018). The nova rose to peak in around 9 days, allowing dedicated pre-maximum spectroscopy on a daily cadence. In Figure 10 we present the evolution of some of the THEA lines during the rise to optical peak. Initially we observe a broad absorption component at a velocity of around -730 km s^{-1} (highlighted in magenta), which disappears in ~ 1 day, as the narrower slow component (at a velocity of -550 km s^{-1}) becomes dominant. While rising to peak, the absorption troughs of the slow component moves redward, receding to a velocity of around -400 km s^{-1} near peak. The implications of this apparent deceleration is discussed in the following sections. A gap in our spectroscopic coverage after peak, followed by secondary maxima, complicates the later spectral evolution and identification of the principal component for this nova.

3.5. Additional conclusions about the early spectral evolution of novae

In this section we list some of the aspects of the spectral evolution we found in novae V906 Car, FM Cir, and the other novae in our sample. For some novae, particularly those with slowly evolving light curves, it was feasible to obtain multiple spectra before the light curve reached its optical peak. In Figure 11 we present the evolution of the velocity of the absorption trough of the slow component of H α and/or H β in comparison to the optical light curves for novae V906 Car, V453 CMA, V5855 Sgr, and V459 Vel. The full evolution of the line profiles for the last three novae are also presented in Figures C.1 and C.2. In addition to the early slow component, followed by—and superimposed upon—a fast component (Section 3.1), we find several other intriguing patterns in their spectral evolution:

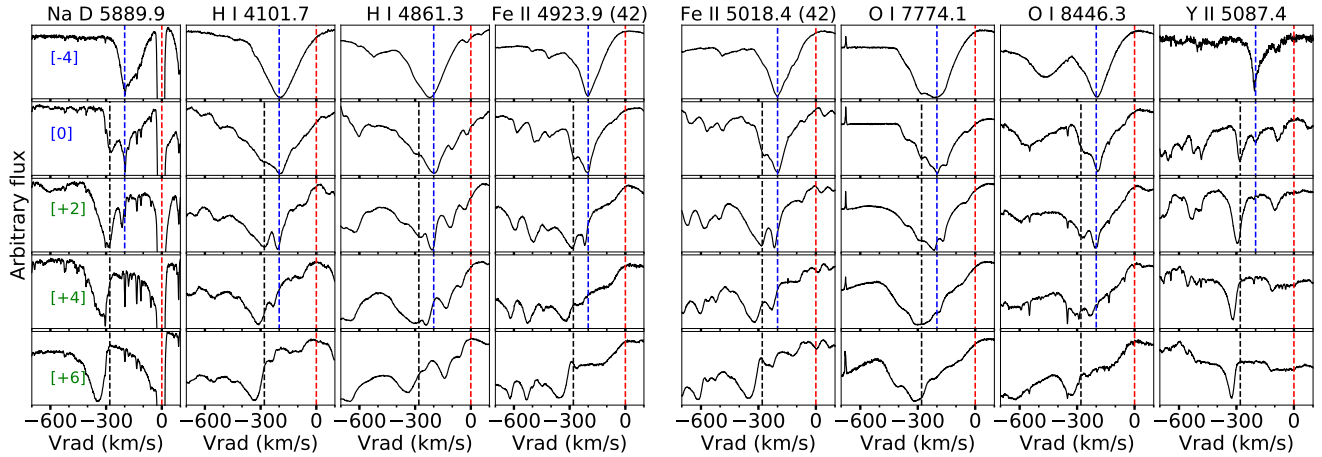


Figure 8. The line profile evolution of some of the Balmer, Fe II (42), and O I lines in comparison with one of the THEA lines and Na I D2 for **nova V906 Car**. The red vertical dashed line represents $v_{\text{rad}} = 0 \text{ km s}^{-1}$ (rest wavelength). The blue vertical dashed line marks a velocity of -200 km s^{-1} highlighting the slow component. The black dashed line marks a velocity of -300 km s^{-1} highlighting the intermediate component.

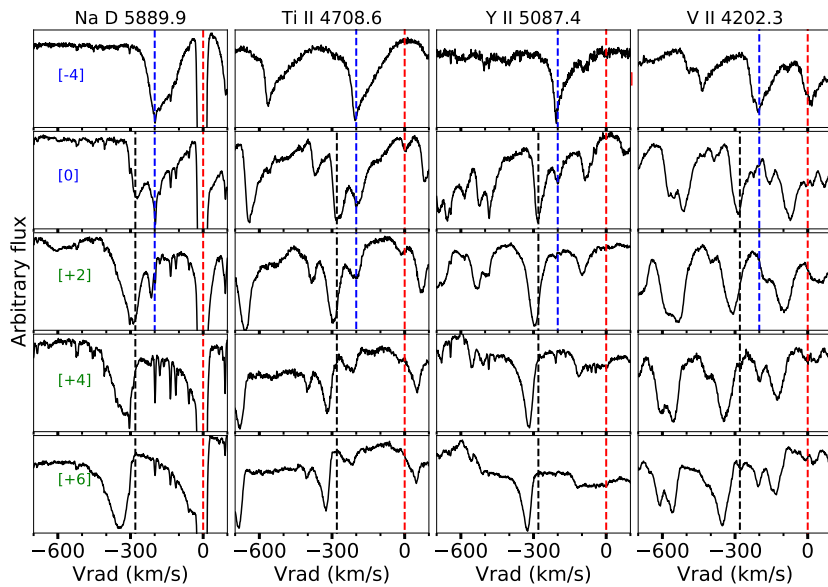


Figure 9. The line profile evolution of a sample of THEA lines plotted in comparison to Na I D2 at 5889.9 \AA for **nova V906 Car**. The red vertical dashed line represents $v_{\text{rad}} = 0 \text{ km s}^{-1}$ (rest wavelength). The blue vertical dashed line marks a velocity of -200 km s^{-1} highlighting the slow component. The black dashed line marks a velocity of -300 km s^{-1} highlighting the intermediate component.

- A pre-maximum deceleration of the slow component. The trough of the blue-shifted absorption feature moves redward while the nova is rising to its peak (Figure 11).
- A gradual post-maximum acceleration of the slow component. After the nova reaches optical peak, the troughs of the blue-shifted absorption fea-

tures of the slow component move blueward. We observed the same acceleration in the intermediate component as well, in nova V906 Car. Nova V5855 Sgr shows a sudden large increase in the velocity of the slow P Cygni absorption component 2 days after peak (see Figure 11). This is likely due to the slow component being replaced by the intermediate component. A distinction be-

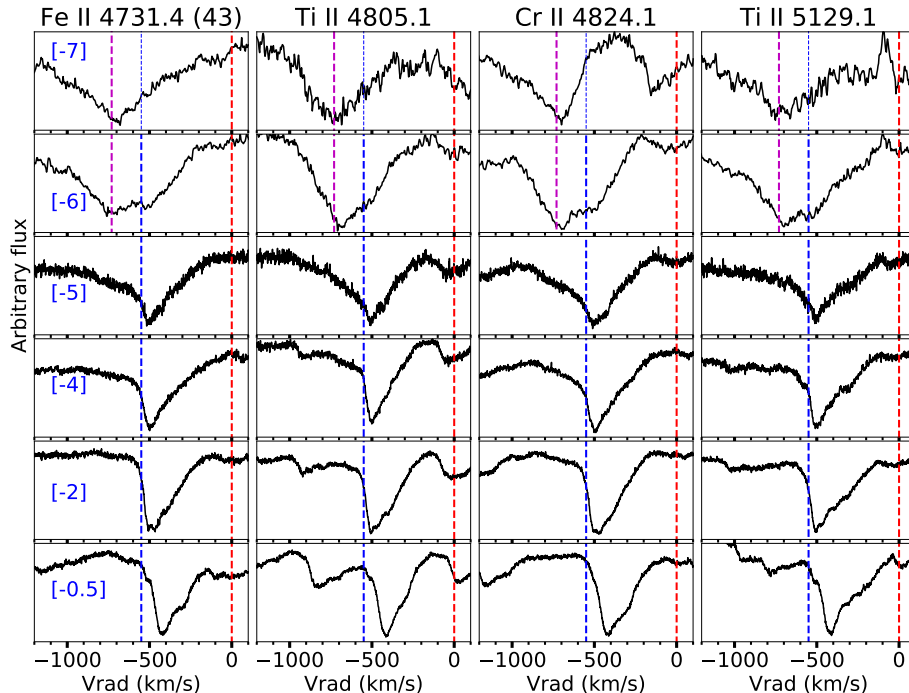


Figure 10. The pre-maximum line profile evolution of a sample of THEA lines for **nova FM Cir**. The red vertical dashed line represents $v_{\text{rad}} = 0 \text{ km s}^{-1}$ (rest wavelength). The blue vertical dashed line marks a velocity of -550 km s^{-1} highlighting the slow component. The magenta vertical dashed line marks a velocity of -730 km s^{-1} . The numbers between brackets are days relative to optical peak.

tween the slow and intermediate components was not feasible for this nova due to the poor cadence. [McLaughlin \(1944\)](#) noted that dedicated monitoring is needed to simultaneously detect the slow and intermediate components.

- A post-maximum acceleration of the fast component. Similar to the other components, the fast component appears to accelerate (the emission line base gradually broadens and the broad absorption feature moves blueward; see Figures 5 and 6). This line broadening has been observed in many novae after peak (see e.g., [Friedjung 2011](#) and references therein),

4. DISCUSSION

4.1. A universal ejection scenario

The co-existence of the pre-maximum P Cygni profile (slow component) on top of the broad emission lines (fast component), and the large velocity difference between these two spectral components, lead us to conclude that there are at least two physically distinct flows. Since all the novae in our sample follow the same spectral evolution, we suggest that this behavior is common and may even be ubiquitous in classical novae.

Our findings here echo the results of [McLaughlin \(1947\)](#), who states:

The broad emissions of the “diffuse-enhanced” system extend across the emission and absorption of the same lines from the principal shell. Nevertheless, the principal absorption remains strong and well defined, without the filling in that would surely occur if the atoms that produce the “diffuse-enhanced” emission were outermost.

McLaughlin concludes that “The ‘diffuse-enhanced’ emission and absorption must be assigned to a P Cygni-like expanding atmosphere close to the central star and wholly inside the principal shell.” Decades worth of progress in spectroscopic observations leave these basic conclusions unchanged. In order for the slow absorption to be superimposed on the broad emission, much of the ejecta associated with the fast or diffuse-enhanced components must be located at smaller radius, compared to the slow or pre-maximum ejecta.

[McLaughlin \(1964\)](#) pictured the two ejections as spheres, with the fast component entirely within the slow component. However, given their relative velocities, the fast component should quickly catch up with and grow beyond the confines of the slow component.

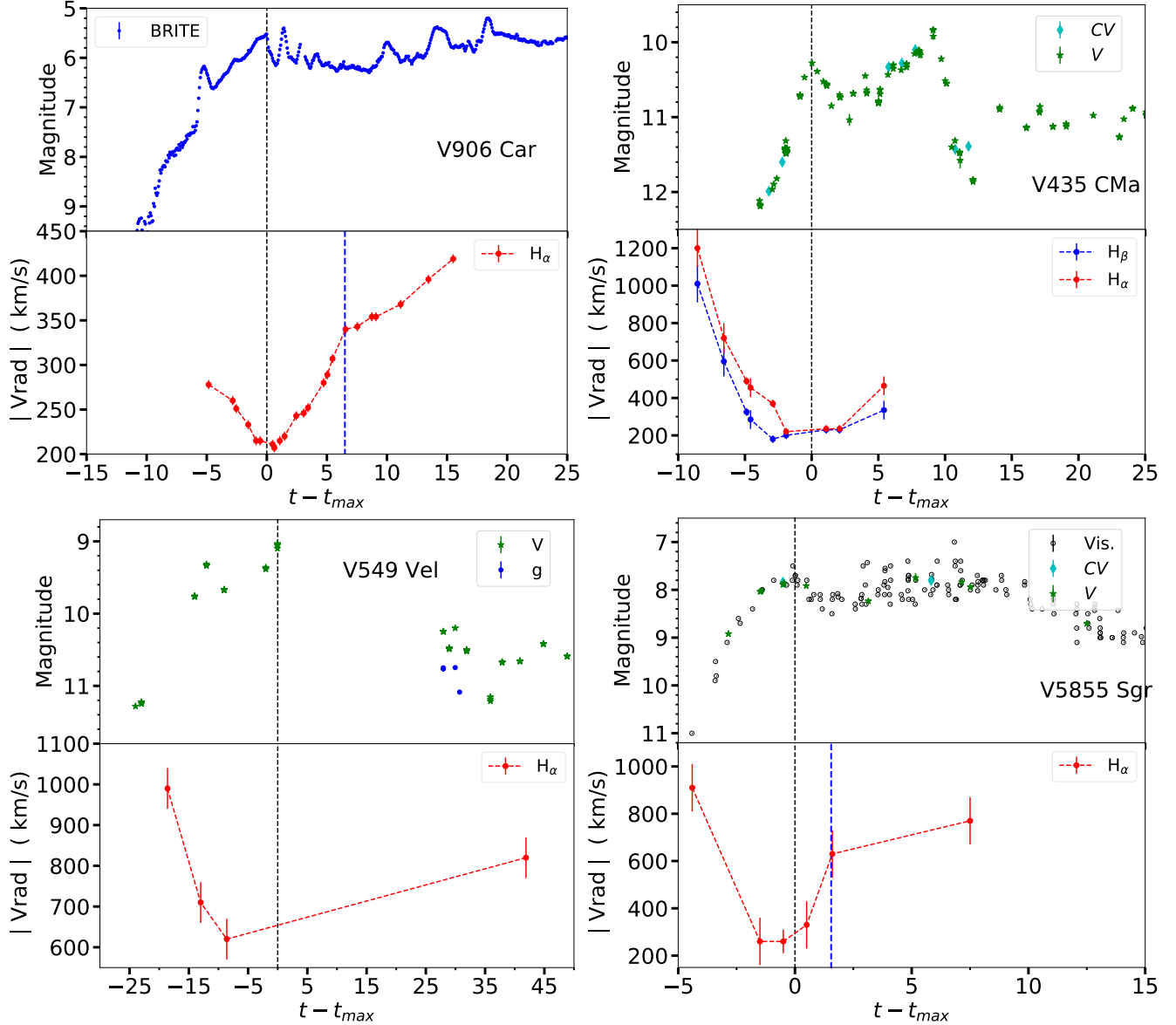


Figure 11. For each of four novae, the V/g -band light curve (*top panel*) is compared with the evolution of velocity for the slow $H\alpha$ and/or $H\beta$ component (*bottom panel*; measured as the velocity of the absorption trough center). Novae V906 Car, V435 CMa, V549 Vel, and V5855 Sgr are shown. The black dashed lines represent the date of the optical peak. For V906 Car we use the BRITE optical light curve from Aydi et al. (2020); all others are from AAVSO/ASAS-SN (§ 2.3). The blue dashed lines in some panels represent the tentative replacement of the slow component by the intermediate component.

Let us take, for example, V906 Car. The slow component expands at $\sim 200 \text{ km s}^{-1}$ and we assume that it is expelled at the beginning of optical rise (11 days before optical peak; Aydi et al. 2020). The fast component is observed to begin expanding ~ 12 days later, a couple of days after peak, at $\sim 1200 \text{ km s}^{-1}$. This implies that the fast component would catch up with the slow component just 2.4 days after the launch of the fast component (i.e., 14.4 days after the start of the optical eruption). The fact that the fast component is not clearly seen to decelerate around this time, and instead actually accel-

erates (Figure 5), implies that some portions of the fast flow continue to freely expand beyond the radius of the slow flow.

Therefore, the spectroscopic observations imply that the two ejections are aspherical, as illustrated in Figure 12. Although the fast flow begins after the expansion of the slow component, it is able to expand relatively freely and unimpeded in the polar directions. Absorption associated with the slow component weakens over time, as the emitting area of the fast component expands beyond the extent of the slow flow.

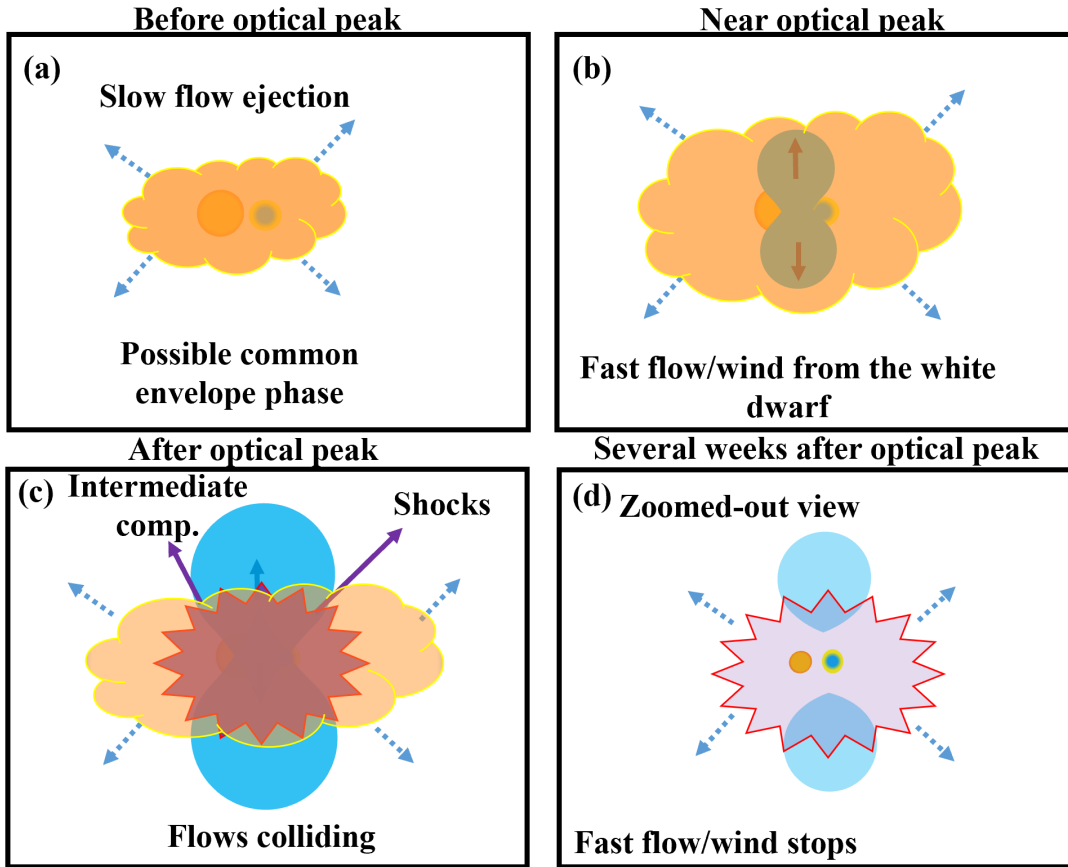


Figure 12. Our proposed universal model of nova ejection: (a) before optical peak the accreted envelope puffs up due to energy output from the thermonuclear reactions, engulfing the system in a common envelope phase and becoming concentrated in the equatorial plane (e.g., Livio et al. 1990; Chomiuk et al. 2014; Sokoloski et al. 2017). This is the slow or pre-maximum component. (b) A continuous fast wind starts, driven by radiation from the ongoing nuclear burning on the surface of the white dwarf (e.g., Bath & Shaviv 1976; Kato & Hachisu 1994). The fast flow could propagate more freely in the polar directions due to the oblate shape of the pre-existing slower ejecta. (c) As the fast flow collides with the slow flow, it leads to shock interaction and physically accelerates the slow ejecta. This interaction could form a shell which sweeps through the slow flow and is the origin of the intermediate spectroscopic component (Friedjung 1987). This same interaction could power the γ -ray and a substantial fraction of the optical emission of the nova (Aydi et al. 2020). (d) Several days/months after optical peak, the continuous ejection of the fast outflow stops, and the ejecta dissipate and become optically thin to the remnant nuclear burning on the white dwarf, observable as a supersoft X-ray source.

Chomiuk et al. (2014), Metzger et al. (2015) and Li et al. (2017b) have suggested a similar scenario to explain high-resolution images, γ -ray emission, and shock formation in novae. Initially, parts of the accreted envelope expand due to the energy of the thermonuclear runaway, and engulf the binary system in a common envelope stage. The binary motion might help to expel the envelope due to frictional drag (e.g., MacDonald et al. 1985; Shankar et al. 1991, though see Kato & Hachisu 1991a,b for another view), or at least direct the ejection, concentrating it in the orbital plane (Livio et al. 1990; Lloyd et al. 1997). This manifests as a slow flow with P Cygni spectral line profiles and velocities $\lesssim 1000$

km s^{-1} , apparent from the earliest times in the eruption (i.e., during the light curve rise to its peak).

The slow flow is followed by a faster wind, which propagates more freely in the bipolar direction since the slower flow is concentrated in the equatorial plane. The origin of the fast flow is possibly a radiation-driven wind from the continuous nuclear burning on the surface of the white dwarf (Bath & Shaviv 1976; Kato & Hachisu 1994). As discussed in Section 4.2, the interaction of the two flows gives rise to high energy emission and additional spectral features.

4.2. *The origin of the intermediate component and the link to γ -ray emitting shocks and optical peak*

McLaughlin (1944) and McLaughlin (1947) pointed out that the intermediate component (principal spectrum) appears a \sim few hours to a couple of days after optical peak and has an intermediate velocity between the slow and fast components. The observed change is quite abrupt and both components (slow and intermediate) co-exist for a few days.

As stated by McLaughlin (1943), the intermediate component originates in a swept-up shell, but it is unclear if it is swept up by shock interaction or radiation pressure:

At this point we must attempt to account for the emergence of the principal spectrum and the disappearance of the pre-maximum one. In Nova Herculis, Russell suggested that an inner and swifter shell of gas swept up the outer one. If that were a unique case we might accept such an interpretation, but it taxes one's credulity to suggest that each nova had two such discrete shells and that the inner one has overtaken the outer one just after maximum light in each case.

One possibility appears to be that the temperature of the inner star has continued to rise, with consequent increase of the radiation pressure which acts upon the thick "shell" from within. This may become so great that it blows the inner layers right through the outer ones... This is admittedly the most conjectural feature of the suggested model.

We argue that, in fact, the shock interaction hypothesis does *not* "tax one's credulity". First, as shown in Section 3, the presence of two flows is common to all the novae in our sample. Second, as discussed in Section 4.1, it is inevitable that the fast component will catch up with the slow component, and given their relative velocities, this should occur soon after the ejection of the fast component. Third, shocks internal to nova ejecta appear to be common. More than 15 novae have been detected with *Fermi*-LAT since 2010 as γ -ray sources (e.g., (Ackermann et al. 2014; Cheung et al. 2016; Franckowiak et al. 2018), and even more as sources of hard X-ray or radio synchrotron emission (e.g., Taylor et al. 1987; Mukai & Ishida 2001; Mukai et al. 2008; Weston et al. 2016). The time of γ -ray detection of novae coincides with their optical peak and therefore, around the same time as the intermediate component emerges. If the intermediate component is the result of the collision of the

fast and slow flow, this could be the same shock interaction responsible for the γ -ray emission.

Friedjung (1987) discussed the formation of the intermediate component in the context of shock interaction between the fast and slow flows. He hypothesizes that the shell created by the shocked material sweeps through the slow flow, and when most of the slow flow is swept up, the slow component disappears. Friedjung (1987) also pointed out that the shell responsible for the intermediate component may lose its internal energy via radiative cooling. Additionally, Friedjung (1987) derived a shock temperature that would produce X-ray emission, and conjectures that it could be absorbed by the dense medium ahead of the shell, explaining the lack of X-ray detection with the limited X-ray facilities at the time.

McLaughlin (1943) noted that the emergence of the intermediate component always occurs around optical peak, so this timing cannot be a coincidence. In this case, correlation may indeed imply causality: the interaction (shock) that creates the intermediate component could also produce the optical peak. This would explain the coincidence between the optical peak and emergence of the intermediate component for all novae. Munari et al. (2017) suggested that the optical light curves of some novae around maximum can be decomposed into one peak from the fireball expansion, followed by a brighter " γ -ray" peak powered by shock interaction. Li et al. (2017b) and Aydi et al. (2020) demonstrated that γ -ray emitting shocks can indeed power a significant fraction of the optical luminosity during the early days of nova eruptions, rivalling the radiative luminosity from the white dwarf.

4.3. *The pre-maximum deceleration*

The deceleration of the slow flow before optical maximum, which we observe in some novae (Figure 11; particularly those characterized by slowly rising light curves), could be explained by two effects. First, it could be an optical depth effect. If the slow flow is homologous (composed of ejecta with a range of velocities, where $v \propto r$), as the slow flow expands, the photosphere will retreat to slower-moving interior layers, leading to a shift of the absorption to lower velocities (Friedjung 1992; Mason et al. 2018).

The second possible explanation is that it is due to a real physical deceleration of the slow flow. Unless the slow flow is ejected with velocities substantially larger than the local escape velocity, the material will quickly decelerate in the combined potential of the secondary and the white dwarf, leading to an observed deceleration in the spectral line profiles. Pejcha et al. (2016) showed that mass ejected through the L2 outer Lagrangian point

could stay bound to the system, depending on a number of parameters such as binary mass ratio, temperature, and degree of co-rotation of the envelope.

Based on the observed velocities of the slow flows in most novae ($\sim 500\text{--}1000\text{ km s}^{-1}$), the average mass of the binary system, and the estimated radius of the photosphere, we can test if the second explanation is plausible. For a total system mass of $1 M_{\odot}$ and a photospheric radius of 10^{13} cm at maximum light (see e.g., Bath & Shaviv 1976; Bath 1978; Kato & Hachisu 1994), the escape velocity from the system would be around 50 km s^{-1} . This value is small compared to the observed velocity of the slow flow near optical peak. In addition, we see a deceleration of around 150 km s^{-1} in FM Cir during a week. This is $\gtrsim 10$ times larger than the expected deceleration based on the gravitational potential of a $\sim 1 M_{\odot}$ binary. All this implies that the optical depth effect must be the main contributor in the apparent velocity deceleration observed before optical peak. Nevertheless, there is a chance that some of the material near the binary system might not reach escape velocities and fall back into the system.

4.4. *The post-maximum acceleration*

We also observe a gradual acceleration in the slow and intermediate components after the optical peak (Figure 11). Again, this is not a new result; for example, Hutchings (1970) pointed out similar movement of absorption components to more extreme blueshifts as the eruption of LV Vul proceeded.

We suggest that this acceleration is caused by interaction with the fast flow. Steinberg & Metzger (2020) show that, as the fast outflow adds momentum to the swept-up shell separating the fast and slow outflow components, this can manifest as an acceleration in the spectral lines of the intermediate velocity component (assuming the latter is generated in the shell).

The fast flow also shows evidence for acceleration as the base of the emission lines broaden with time and the accompanying absorptions increase in velocity (see Figure 5). The broadening of the fast spectroscopic component can be explained as a wind whose velocity increases with time, as expected for nova radiation-driven winds (Kato & Hachisu 1994).

4.5. *The origin of the THEA lines*

In Figure 9 we showed that the THEA lines of nova V906 Car exhibit a slow (pre-maximum) component and an intermediate component, essentially identical to the velocities and evolution demonstrated in the H I, Fe II, O I, and Na I lines (Figure 8). Therefore, the THEA absorptions originate from the same body of gas respon-

sible for the P Cygni profiles in prominent lines, which we associate with the slow nova ejecta.

The THEA lines observed in nova FM Cir (Figure 10) shows an apparent deceleration by around 150 km s^{-1} during the rise to optical peak. In addition, the lines appear to be broader initially and they become more narrow as the nova rises to peak. Again, this mimics the evolution of more prominent lines associated with the slow ejecta, like Fe II.

As discussed in §3.3.4, no fast component is associated with the THEA lines. Although this could be an optical depth effect (i.e., the THEA lines are too weak to be detected in the fast flow), it is possible that this observation denotes a real absence. The THEA lines are s-process elements and therefore it is unlikely that they are synthesized during the thermonuclear runaway. The THEA elements that are accreted onto the white dwarf throughout the years prior to the nova eruption might selectively diffuse into the white dwarf interior (Williams et al. 2008). It is therefore possible that these elements are freshly accreted onto the white dwarf or that they still reside in the accretion disk prior to the eruption and thus are ejected during the early common envelope phase.

4.6. *Alternative scenarios*

In this section we explore alternative explanations for the origin of the different absorption systems.

4.6.1. *Circumbinary material?*

As mentioned in Section 1.2, Williams et al. (2008) and Williams & Mason (2010) suggested a circumbinary reservoir as the source of the THEA lines. However, these studies missed the presence of similar low-velocity components in the H I, Fe II, and O I lines during the pre-maximum stage. This suggests that the THEA lines are associated with the nova ejecta rather than a circumbinary reservoir. If the THEA lines and the slow, pre-maximum P Cygni profiles of H I, Fe II, and O I all originate in a pre-existing circumbinary reservoir, then there would be no features in the pre-maximum spectra to explain and associate with the rise to peak phase, when the nova brightness increases by 8 to 15 magnitudes.

Similar to the other lines in the spectra, the THEA lines show deceleration during the rise to optical peak (§3.4), which is consistent with a photosphere receding through expanding ejecta (§4.3), rather than a pre-existing circumbinary reservoir of gas. Before eruption and in its early stages, we would expect CSM to exhibit constant velocity. In later stages, Williams et al. (2008); Williams & Mason (2010) used the *acceleration* of the

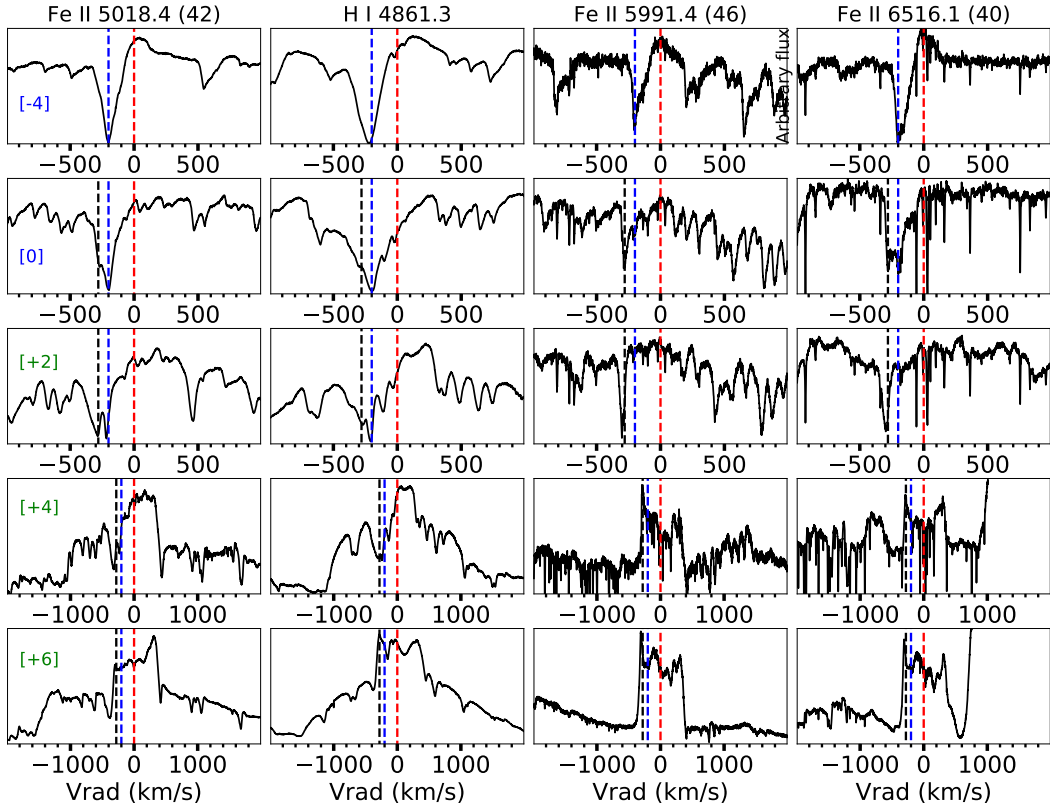


Figure 13. The line profile evolution of a sample of Fe II 5018 Å and H β in comparison Fe II 5991 and 6516 Å for nova V906 Car. The red vertical dashed line represents $v_{\text{rad}} = 0 \text{ km s}^{-1}$ (rest wavelength). The blue vertical dashed line marks a velocity of -200 km s^{-1} highlighting the slow component. The black dashed line marks a velocity of -300 km s^{-1} highlighting the intermediate component. The top three panels extend between -1000 km s^{-1} and 1000 km s^{-1} while the bottom two panels extend between -2000 km s^{-1} and 2000 km s^{-1} to show the fast component.

THEA lines observed post-maximum to argue for a circumbinary origin, with the CSM accelerated outward by the radiation pressure from the white dwarf.

Williams (2012, 2013) argues that the intermediate component (and potentially the slow component), along with the THEA lines, are ablated/irradiated from the secondary star, rather than originating on the white dwarf. He cites as evidence that the velocities of these components are consistent with the escape velocities of the secondary star (\sim a few hundreds km s^{-1}). While this is true for slow novae, faster novae such as ASASSN-19qv and V1707 Sco show pre-maximum P Cygni profiles with absorption troughs at velocities $\gtrsim 1000\text{--}2000 \text{ km s}^{-1}$, much higher than the escape velocities of the secondary star (see Figure 2). In addition, we observe a correlation between the velocities of the slow and fast flows with that of the speed class of the nova (see the marked velocities in Figures 1, and 2). McLaughlin (1944) also points out that the fast component always has around twice the velocity of the intermediate component (see also Gallagher & Starrfield 1978).

This means that both the slow/intermediate flows and their velocities are associated with the eruption and not with the secondary star.

The first spectra of nova FM Cir show a component in the THEA lines at around 800 km s^{-1} (marked by magenta lines in Figure 10) co-existing with the slow component (550 km s^{-1}) before disappearing in one day. The large velocity and behavior of this component is also not consistent with a pre-existing circumbinary reservoir. The origin of this early component could be early ejection of a small body of gas during the TNR. This low density body of gas dissipates rapidly before the bulk of the ejecta expands and engulf the binary. We see a similar behaviour in the early spectra of nova V435 CMa (Figure C.1).

Recently, McLoughlin et al. (2020) suggested the presence of a circumbinary disk rich with Fe and O in nova V906 Car. Their evidence consists of particular emission lines of Fe II at 5991 Å (46), 6432 Å (40), 6456 Å (74), and 6516 Å (40), in addition to [O I] 6300 Å, which are characterized by double-peaked profiles and mod-

est expansion velocities ($\text{FWZI} \approx 900 \text{ km s}^{-1}$). These lines do not develop a broad emission component ($\text{FWZI} \approx 2500 \text{ km s}^{-1}$) like the other lines in the spectrum, such as H I, and other transitions of O I and Fe II (42). McLoughlin et al. associate these double-peaked emission lines with a circumbinary disk and suggest that this disk could also be responsible for the THEA lines.

In Figure 13 we plot two of these lines in comparison with H β and Fe II 5018 Å (42). All four lines show “slow component” P Cygni profiles before optical peak, as do other lines in the spectrum. After optical peak, all of the lines also develop the intermediate component. A few days after optical peak, the Fe II (40) and (46) lines develop a double-peaked narrow emission, but not a fast component. The narrow double-peaked emission is not unique to these lines and is present in the other lines in the spectrum, such as the Balmer and Fe II (42) lines, but these other lines are superimposed on top of a broad emission (see also Figures 6). The spectral evolution of the lines presented in McLoughlin et al. (2020) is then similar to other prominent lines associated with the ejecta, and therefore it is reasonable to associate them with the slow flow rather than a circumbinary disk. The slow flow could propagate aspherically, leading to the observed double peak in the slow component emission profiles.

One explanation for the absence of a fast component in the Fe II (40 & 46) multiplet lines could be the f -value (oscillator strength) of these transitions. The f -values of the Fe II (42) multiplet transitions are $\sim 10^{-3} - 10^{-2}$, while the f -values of the Fe II (40 & 46) multiplets are $\sim 10^{-5}$. The 2–3 orders of magnitude smaller f -values for the (40 & 46) multiplets could result in relatively weak, and possibly undetectable, broad emission lines produced by the lower-density fast wind.

4.6.2. A single ballistic ejection?

Shore et al. (2011, 2013, 2016) and Mason et al. (2018, 2020) model nova line profiles as a single biconical and clumpy ejection. When the (pseudo)photosphere recedes through the homologously expanding ejecta, lines can appear to decelerate. On the other hand, lines can appear to accelerate if a recombination wave sweeps outward through the ejecta (Shore et al. 2011). Mason et al. (2018) point out that some absorption components are present at the same velocities in earlier spectra (in low ionization lines) and later spectra (in high excitation lines). This led them to conclude that the ejecta are stationary in velocity, characterized by a single ballistic explosion. In this scenario, shock signatures can be produced at early times if the ejecta are expelled with a large range in velocities. Clumps will crash into one an-

other as the flow relaxes to homologous expansion (Shore et al. 2013).

A single ballistic ejection cannot explain the early spectral evolution of novae: specifically, a relatively slow absorption component superimposed on fast emission. As pointed out decades ago by McLaughlin, the fact that the slow component is seen in absorption necessitates that it is external to the fast component—and this, in turn, necessitates that the fast component must have been ejected after the slow component (§4.1). Mason et al. (2018, 2020) did not tackle the early spectral evolution of the novae they consider; instead, their observations are obtained at later stages (more than one hundred days after eruption). During this late stage, the ejecta probably are expanding ballistically, after the mass loss has ceased. On the other hand, Hauschildt et al. (1994, 1995, 1996, 1997) were able to explain many aspects of the early spectra of novae with a single ballistic ejection, but their models always predict lines composed of a single P Cygni profile; they provide no explanation for the slow/intermediate component superimposed on top of the fast component.

In addition, in a scenario where impulsively ejected clumps of different velocities collide to produce the shocks and γ -rays, these collisions should occur immediately, and last no longer than the impulsive ejection itself. Instead, we see that gamma-rays do not appear until optical maximum and can remain detectable for weeks (e.g., Cheung et al. 2016). In order to explain the prolonged periods of gamma-ray detection and other shock signatures, mass ejection itself must be prolonged in time.

While a photosphere receding through homologously expanding ejecta can reveal slower spectral components with time, and while a recombination wave moving outward through the ejecta might reveal faster components, neither phenomenon can explain the sudden appearance of an intermediate-velocity component. Take, for example, V906 Car. Its intermediate component appears at optical peak (day ~ 0 ; Figure 8), around the same time as the fast component (Figure 5). The fact that the fast component is visible would imply, in the ballistic outflow scenario, that the recombination wave has reached the outer extent of the ejecta. Meanwhile, the slow component is also present (Figure 8), which would imply that inner ejecta are contributing to the line profile. The appearance of the intermediate component cannot be explained by changes in opacity or ionization state of the ejecta, and therefore implies an actual change in the ejecta configuration (i.e., a new swept-up shell). In addition, the acceleration of spectral components after optical peak (e.g., Figure 11) is difficult to explain as

a recombination front, given that the fast component tracing the outer ejecta is present in the line profile.

5. SUMMARY AND CONCLUSIONS

Based on the near-peak evolution of the Balmer line profiles of all the novae in our sample and the spectral evolution of novae V906 Car and FM Cir, we reached the following conclusions:

- All 12 novae show the same spectral evolution: before optical peak, the line profiles are dominated by P Cygni profiles characterized by slow velocities ($\lesssim 1000 \text{ km s}^{-1}$). After optical peak, a broad emission base emerges characterized by faster velocities (more than double that of the slow component), while the pre-existing P Cygni profile is superimposed on top of the broad emission component.
- The co-existence of the fast and slow spectral components (slow P Cygni superimposed on top of the fast component), the large difference in velocity between them, and the abrupt transition of the spectral profiles in a matter of \sim a day indicate the presence of at least two physically distinct flows. It also indicates that the faster flow originates from inside the slower one.
- For novae with multiple observations before and after peak, we notice that the spectral components also show similar velocity evolution. The absorption trough of the slow component decelerates until peak, then accelerates. The fast component accelerates once it appears.
- The THEA lines in nova V906 Car show the same spectral evolution of the Balmer, Fe II, and O I near optical peak, except they do not show the emergence of a fast component. In FM Cir, THEA lines in the pre-maximum spectra appear to decelerate during the rise to peak. We argue that the THEA lines are associated with the nova slow flow, rather than a pre-existing circumbinary reservoir of gas.
- The fast, internal outflow must be launched after the slow outflow, but even so, it is expected to quickly catch up with the slow outflow. However, the fast component persists in the spectrum long after the time when collision is expected, implying that the ejecta are likely aspherical and the fast flow expands relatively unimpeded in some directions.
- For nova V906 Car we detect the emergence of an intermediate component with slightly bluer velocities compared to the slow component. This

intermediate component replaces the slow, pre-maximum one a few days after optical peak. We suggest that this intermediate component originates in a shell formed by the collision of the slow and fast flows.

- Since all of the novae in our sample follow the same spectral evolution, we suggest a common scenario to explain the observations. The scenario consists of an initial ejection of the slow flow, which could be expelled preferentially in the orbital plane during a common envelope phase. This is followed by a fast flow—likely a radiation pressure driven wind—which sweeps through the slow flow and causes it to accelerate.
- The shocks formed by the interaction between these two flows could also be responsible for the γ -ray emission observed in some novae, and may power a significant part of the optical emission of the nova, contributing to its optical peak. This can help explain the coincidence of timing commonly seen in novae: that the fast and intermediate component appear just around optical maximum.

The γ -ray luminosities of novae have been shown to span at least two orders of magnitude (Franckowiak et al. 2018), but the link between shock luminosity and nova properties—and the cause of this diversity in γ -ray luminosity—remain poorly understood (e.g., Finzell et al. 2018; Franckowiak et al. 2018). To first order, we might expect shock luminosity to be determined by the density and velocity of the ejecta (Metzger et al. 2015). Since we can measure the differential velocity between the fast and slow flows with optical spectroscopy, we can use this to estimate the luminosity of the shock—if we know the distance to the nova and have an estimate of the mass of the ejecta from e.g., radio observations (Chomiuk et al. 2012, 2014; Weston et al. 2016; Aydi et al. 2020). Future work should be dedicated to making such observations for a large sample of novae, in order to test theories about nova shocks and γ -ray production, and understand the diversity of shock luminosities observed for γ -ray detected novae.

In this paper we proposed a qualitative scenario explaining the spectral evolution of novae near maximum light. The next step would be to construct a quantitative model with radiation hydrodynamical simulations to attempt to describe the observed spectra. Given the modest size of our current sample of early nova spectroscopy and the observed diversity of novae, more pre-maximum spectral observations will also inform our understanding of mass ejection in novae.

ACKNOWLEDGMENTS

EA, LC, JL-M, and KVS acknowledge NSF award AST-1751874, NASA award 11-Fermi 80NSSC18K1746, and a Cottrell fellowship of the Research Corporation. JS was supported by the Packard Foundation. LI was supported by grants from VILLUM FONDEN (project number 16599 and 25501). DAHB gratefully acknowledges the receipt of research grants from the National Research Foundation (NRF) of South Africa. CSK and BJS are supported by NSF grant AST-1907570/AST-1908952. CSK is also supported by NSF grants AST-1515927 and AST-181440. BJS is also supported by NSF grants AST-1920392 and AST-1911074. PAW kindly acknowledges the National Research Foundation and the University of Cape Town. FMW acknowledges support of the US taxpayers through NSF grant 1611443.

ASAS-SN thanks the Las Cumbres Observatory and its staff for its continuing support of the ASAS-SN project. ASAS-SN is supported by the Gordon and Betty Moore Foundation through grant GBMF5490 to the Ohio State University and NSF grant AST-1515927. Development of ASAS-SN has been supported by NSF grant AST-0908816, the Mt. Cuba Astronomical Foundation, the Center for Cosmology and AstroParticle Physics at the Ohio State University, the Chinese Academy of Sciences South America Center for

Astronomy (CASSACA), the Villum Foundation, and George Skestos.

We thank Robert E. Williams for useful comments and discussion. We thank Kristen Dage and Chelsea Harris for useful comments and support during this work. We thank the AAVSO observers from around the world who contributed their magnitude measurements to the AAVSO International Database used in this work. We acknowledge all the ARAS observers for their optical spectroscopic observations which complement our data. This work is based on observations obtained at the Southern Astrophysical Research (SOAR) telescope, which is a joint project of the Ministério da Ciência, Tecnologia, Inovações e Comunicações (MCTIC) do Brasil, the U.S. National Optical Astronomy Observatory (NOAO), the University of North Carolina at Chapel Hill (UNC), and Michigan State University (MSU). A part of this work is based on observations made with the Southern African Large Telescope (SALT), with the Large Science Programme on transients 2018-2-LSP-001 (PI: DAHB). This work is also partly based on observations collected at the European Organisation for Astronomical Research in the Southern Hemisphere under ESO programme(s) PPP.C-NNNN(R). This paper includes data gathered with the 6.5 meter Magellan Telescopes located at Las Campanas Observatory, Chile. Polish participation in SALT is funded by grant no. MNiSW DIR/WK/2016/07.

REFERENCES

- Abdo, A. A., Ackermann, M., Ajello, M., et al. 2010, *Science*, 329, 817
- Ackermann, M., Ajello, M., Albert, A., et al. 2014, *Science*, 345, 554
- Arai, A., Kawakita, H., Shinnaka, Y., & Tajitsu, A. 2016, *ApJ*, 830, 30
- Aydi, E., Chomiuk, L., Sokolovsky, K. V., & Steinberg, E. 2020, *Nature Astronomy*, 2, 697
- Aydi, E., Orio, M., Beardmore, A. P., et al. 2018, *MNRAS*, 480, 572
- Aydi, E., Chomiuk, L., Strader, J., et al. 2019, arXiv e-prints, arXiv:1903.09232
- Ballester, P. 1992, in *European Southern Observatory Conference and Workshop Proceedings*, Vol. 41, European Southern Observatory Conference and Workshop Proceedings, ed. P. J. Grosbøl & R. C. E. de Ruijsscher, 177
- Barnes, S. I., Cottrell, P. L., Albrow, M. D., et al. 2008, in *Proc. SPIE*, Vol. 7014, *Ground-based and Airborne Instrumentation for Astronomy II*, 70140K
- Bath, G. T. 1978, *MNRAS*, 182, 35
- Bath, G. T., & Shaviv, G. 1976, *MNRAS*, 175, 305
- Bernstein, R., Shtetman, S. A., Gunnels, S. M., Mochnacki, S., & Athey, A. E. 2003, in *Proc. SPIE*, Vol. 4841, *Instrument Design and Performance for Optical/Infrared Ground-based Telescopes*, ed. M. Iye & A. F. M. Moorwood, 1694–1704
- Bramall, D. G., Sharples, R., Tyas, L., et al. 2010, in *Proc. SPIE*, Vol. 7735, *Ground-based and Airborne Instrumentation for Astronomy III*, 77354F
- Bramall, D. G., Schmoll, J., Tyas, L. M. G., et al. 2012, in *Proc. SPIE*, Vol. 8446, *Ground-based and Airborne Instrumentation for Astronomy IV*, 84460A
- Buckley, D. A. H., Swart, G. P., & Meiring, J. G. 2006, in *Proc. SPIE*, Vol. 6267, *Society of Photo-Optical Instrumentation Engineers (SPIE) Conference Series*, 62670Z
- Cheung, C. C., Jean, P., Shore, S. N., et al. 2016, *ApJ*, 826, 142

- Chomiuk, L., Krauss, M. I., Rupen, M. P., et al. 2012, *ApJ*, 761, 173
- Chomiuk, L., Linford, J. D., Yang, J., et al. 2014, *Nature*, 514, 339
- Chomiuk, L., Strader, J., Stanek, K. Z., et al. 2018, *The Astronomer's Telegram*, 11132, 1
- Chugai, N. N., & Danziger, I. J. 1994, *MNRAS*, 268, 173
- Chugai, N. N., Danziger, I. J., & della Valle, M. 1995, *MNRAS*, 276, 530
- Clemens, J. C., Crain, J. A., & Anderson, R. 2004, in *Proc. SPIE*, Vol. 5492, *Ground-based Instrumentation for Astronomy*, ed. A. F. M. Moorwood & M. Iye, 331–340
- Clerke, A. M. 1892, *The Observatory*, 15, 334
- Crause, L. A., Sharples, R. M., Bramall, D. G., et al. 2014, in *Proc. SPIE*, Vol. 9147, *Ground-based and Airborne Instrumentation for Astronomy V*, 91476T
- Crawford, S. M., Still, M., Schellart, P., et al. 2010, in *Society of Photo-Optical Instrumentation Engineers (SPIE) Conference Series*, Vol. 7737, *Society of Photo-Optical Instrumentation Engineers (SPIE) Conference Series*, 25
- Dekker, H., D'Odorico, S., Kaufer, A., Delabre, B., & Kotzlowski, H. 2000, in *Society of Photo-Optical Instrumentation Engineers (SPIE) Conference Series*, Vol. 4008, *Optical and IR Telescope Instrumentation and Detectors*, ed. M. Iye & A. F. Moorwood, 534–545
- Dessart, L., Hillier, D. J., Audit, E., Livne, E., & Waldman, R. 2016, *MNRAS*, 458, 2094
- Downes, R. A., & Duerbeck, H. W. 2000, *AJ*, 120, 2007
- Dubus, G., Campbell, R., Kern, B., Taam, R. E., & Spruit, H. C. 2004, *MNRAS*, 349, 869
- Finzell, T., Chomiuk, L., Metzger, B. D., et al. 2018, *ApJ*, 852, 108
- Fox, O. D., Silverman, J. M., Filippenko, A. V., et al. 2015, *MNRAS*, 447, 772
- Frankowiak, A., Jean, P., Wood, M., Cheung, C. C., & Buson, S. 2018, *A&A*, 609, A120
- Freudling, W., Romaniello, M., Bramich, D. M., et al. 2013, *A&A*, 559, A96
- Friedjung, M. 1966a, *MNRAS*, 131, 447
- . 1966b, *MNRAS*, 132, 143
- . 1966c, *MNRAS*, 132, 317
- . 1987, *A&A*, 180, 155
- . 1992, *A&A*, 262, 487
- . 2011, *A&A*, 536, A97
- Froning, C. S. 2005, in *Astronomical Society of the Pacific Conference Series*, Vol. 330, *The Astrophysics of Cataclysmic Variables and Related Objects*, ed. J. M. Hameury & J. P. Lasota, 81
- Gallagher, J. S., & Starrfield, S. 1978, *ARA&A*, 16, 171
- Gangopadhyay, A., Turatto, M., Benetti, S., et al. 2020, *arXiv e-prints*, arXiv:2008.10482
- Guido, E., Howes, N., Nicolini, M., et al. 2013, *IAUC*, 9265, 1
- Hauschildt, P. H., Baron, E., Starrfield, S., & Allard, F. 1996, *ApJ*, 462, 386
- Hauschildt, P. H., Shore, S. N., Schwarz, G. J., et al. 1997, *ApJ*, 490, 803
- Hauschildt, P. H., Starrfield, S., Austin, S., et al. 1994, *ApJ*, 422, 831
- Hauschildt, P. H., Starrfield, S., Shore, S. N., Allard, F., & Baron, E. 1995, *ApJ*, 447, 829
- Hoard, D. W., Long, K. S., Howell, S. B., et al. 2014, *ApJ*, 786, 68
- Hutchings, J. B. 1970, *PASP*, 82, 603
- Iijima, T., Rosino, L., & della Valle, M. 1998, *A&A*, 338, 1006
- Itagaki, K., Nakano, S., Kojima, T., et al. 2019, *Central Bureau Electronic Telegrams*, 4667, 1
- Jacques, C., Amaral, L., Colesanti, C., et al. 2019, *Transient Name Server Discovery Report*, 2019-1337, 1
- Jerkstrand, A., Maeda, K., & Kawabata, K. S. 2020, *Science*, 367, 415
- Kafka, S. 2020, *Observations from the AAVSO International Database*, <https://www.aavso.org>
- Kato, M., & Hachisu, I. 1991a, *ApJ*, 373, 620
- . 1991b, *ApJ*, 383, 761
- . 1994, *ApJ*, 437, 802
- Kaufer, A., Stahl, O., Tubbesing, S., et al. 1999, *The Messenger*, 95, 8
- Kniazhev, A. Y., Gvaramadze, V. V., & Berdnikov, L. N. 2016, *MNRAS*, 459, 3068
- Kochanek, C. S., Shappee, B. J., Stanek, K. Z., et al. 2017, *PASP*, 129, 104502
- Li, K.-L., Chomiuk, L., & Strader, J. 2017a, *The Astronomer's Telegram*, 10977, 1
- Li, K.-L., Metzger, B. D., Chomiuk, L., et al. 2017b, *Nature Astronomy*, 1, 697
- Li, K.-L., Aydi, E., Sokolovsky, K., et al. 2019, *The Astronomer's Telegram*, 13116, 1
- Livio, M., Shankar, A., Burkert, A., & Truran, J. W. 1990, *ApJ*, 356, 250
- Lloyd, H. M., O'Brien, T. J., & Bode, M. F. 1997, *MNRAS*, 284, 137
- MacDonald, J., Fujimoto, M. Y., & Truran, J. W. 1985, *ApJ*, 294, 263
- Martin, P., & Dubus, G. 2013, *A&A*, 551, A37
- Mason, E., Shore, S. N., De Gennaro Aquino, I., et al. 2018, *ApJ*, 853, 27

- Mason, E., Shore, S. N., Kuin, P., & Bohlson, T. 2020, arXiv e-prints, arXiv:2001.11747
- McLaughlin, D. B. 1943, *Publications of Michigan Observatory*, 8, 149
- . 1944, *Popular Astronomy*, 52, 109
- . 1945, *PASP*, 57, 69
- . 1947, *PASP*, 59, 244
- . 1964, *Annales d'Astrophysique*, 27, 450
- McLoughlin, D., Blundell, K. M., & Lee, S. 2020, *MNRAS*, 494, 743
- Metzger, B. D., Finzell, T., Vurm, I., et al. 2015, *MNRAS*, 450, 2739
- Molaro, P., Izzo, L., Bonifacio, P., et al. 2020, *MNRAS*, 492, 4975
- Mukai, K., & Ishida, M. 2001, *ApJ*, 551, 1024
- Mukai, K., Orio, M., & Della Valle, M. 2008, *ApJ*, 677, 1248
- Munari, U., Hamsch, F.-J., & Frigo, A. 2017, *ArXiv e-prints* 1703.09017, arXiv:1703.09017
- Nakamura, Y., Soma, M., Schmeer, P., Kiyota, S., & Strader, J. 2018, *Central Bureau Electronic Telegrams*, 4499, 1
- Nakano, S., Pearce, A., & Ayani, K. 2016, *IAUC*, 9284, 5
- Nelson, T., Donato, D., Mukai, K., Sokoloski, J., & Chomiuk, L. 2012, *ApJ*, 748, 43
- Nelson, T., Mukai, K., Li, K.-L., et al. 2019, *ApJ*, 872, 86
- Nyamai, M. M., Chomiuk, L., Ribeiro, V. A. R. M., et al. 2020, *MNRAS*
- O'Brien, T. J., & Bode, M. F. 2008, in *Classical Novae Cambridge Astrophysics Series*, No. 43, Cambridge: Cambridge University Press, ed. E. by M.F. Bode & A. Evans., 285–306
- O'Donoghue, D., Buckley, D. A. H., Balona, L. A., et al. 2006, *MNRAS*, 372, 151
- Pavana, M., Raj, A., Bohlson, T., et al. 2020, *MNRAS*, 495, 2075
- Payne-Gaposchkin, C. H. P. 1957, *The galactic novae*. Amsterdam, North-Holland Pub. Co.; New York, Interscience Publishers
- Pejcha, O. 2009, *ApJL*, 701, L119
- Pejcha, O., Metzger, B. D., & Tomida, K. 2016, *MNRAS*, 461, 2527
- Poggiani, R. 2008, *NewA*, 13, 557
- Rupen, M. P., Dhawan, V., & Mioduszewski, A. 2001, *IAUC*, 7717, 1
- Russell, H. N. 1936, *PASP*, 48, 29
- Sakurai, Y., Nakano, S., Kiyota, S., et al. 2018, *Central Bureau Electronic Telegrams*, 4530, 1
- Seach, J., Pearce, A., Chapman, A., et al. 2018, *Central Bureau Electronic Telegrams*, 4482, 1
- Shankar, A., Livio, M., & Truran, J. W. 1991, *ApJ*, 374, 623
- Shappee, B. J., Prieto, J. L., Grupe, D., et al. 2014, *ApJ*, 788, 48
- Shara, M. 1995, *The Structure of Nova Shells*, HST Proposal, ,
- Shectman, S. A., & Johns, M. 2003, in *Proc. SPIE*, Vol. 4837, *Large Ground-based Telescopes*, ed. J. M. Oschmann & L. M. Stepp, 910–918
- Shore, S. N. 2014, in *Astronomical Society of the Pacific Conference Series*, Vol. 490, *Stellar Novae: Past and Future Decades*, ed. P. A. Woudt & V. A. R. M. Ribeiro, 145
- Shore, S. N., Augusteijn, T., Ederoclite, A., & Uthas, H. 2011, *A&A*, 533, L8
- Shore, S. N., De Gennaro Aquino, I., Schwarz, G. J., et al. 2013, *A&A*, 553, A123
- Shore, S. N., Mason, E., Schwarz, G. J., et al. 2016, *A&A*, 590, A123
- Smith, N., Chornock, R., Li, W., et al. 2008, *ApJ*, 686, 467
- Sokoloski, J. L., Lawrence, S., Crotts, A. P. S., & Mukai, K. 2017, *arXiv e-prints*, arXiv:1702.05898
- Sokolovsky, K. V., Mukai, K., Chomiuk, L., et al. 2020, *MNRAS*, arXiv:2007.07885
- Stahl, O., Kaufer, A., & Tubbesing, S. 1999, in *Astronomical Society of the Pacific Conference Series*, Vol. 188, *Optical and Infrared Spectroscopy of Circumstellar Matter*, ed. E. Guenther, B. Stecklum, & S. Klose, 331
- Stanek, K. Z. 2019, *Transient Name Server Discovery Report*, 2019-1142, 1
- Stanek, K. Z., & Kochanek, C. S. 2019, *Transient Name Server Discovery Report*, 2019-774, 1
- Stanek, K. Z., Kochanek, C. S., Shields, J. V., et al. 2017, *The Astronomer's Telegram*, 10772, 1
- Stanek, K. Z., Holoiu, T. W.-S., Kochanek, C. S., et al. 2018, *The Astronomer's Telegram*, 11454
- Starrfield, S., Iliadis, C., & Hix, W. R. 2008, in *Classical Novae*, ed. E. by M.F. Bode & A. Evans, 77–101
- Starrfield, S., Iliadis, C., & Hix, W. R. 2016, *PASP*, 128, 051001
- Steinberg, E., & Metzger, B. D. 2020, *MNRAS*, 491, 4232
- Strope, R. J., Schaefer, B. E., & Henden, A. A. 2010, *AJ*, 140, 34
- Sytov, A. Y., Kaigorodov, P. V., Bisikalo, D. V., Kuznetsov, O. A., & Boyarchuk, A. A. 2007, *Astronomy Reports*, 51, 836
- Taam, R. E., & Spruit, H. C. 2001, *ApJ*, 561, 329
- Tanaka, J., Nogami, D., Fujii, M., Ayani, K., & Kato, T. 2011, *PASJ*, 63, 159
- Taylor, A. R., Seaquist, E. R., Hollis, J. M., & Pottasch, S. R. 1987, *A&A*, 183, 38

- Teyssier, F. 2019, Contributions of the Astronomical Observatory Skalnaté Pleso, 49, 217
- Tody, D. 1986, in Society of Photo-Optical Instrumentation Engineers (SPIE) Conference Series, Vol. 627, Instrumentation in astronomy VI, ed. D. L. Crawford, 733
- Tokovinin, A., Fischer, D. A., Bonati, M., et al. 2013, PASP, 125, 1336
- Warmels, R. H. 1992, in Astronomical Society of the Pacific Conference Series, Vol. 25, Astronomical Data Analysis Software and Systems I, ed. D. M. Worrall, C. Biemesderfer, & J. Barnes, 115
- Warner, B. 2008, in Classical Novae, ed. M. F. Bode & A. Evans, 16–33
- Wee, J., Blagorodnova, N., Penprase, B. E., et al. 2020, arXiv e-prints, arXiv:2006.14336
- Weston, J. H. S., Sokoloski, J. L., Metzger, B. D., et al. 2016, MNRAS, 457, 887
- Williams, R. 2013, AJ, 146, 55
- Williams, R., & Mason, E. 2010, Ap&SS, 327, 207
- Williams, R., Mason, E., Della Valle, M., & Ederoclite, A. 2008, ApJ, 685, 451
- Williams, R. E. 2012, AJ, 144, 98
- Wolf, W. M., Bildsten, L., Brooks, J., & Paxton, B. 2013, ApJ, 777, 136
- Woudt, P. A., Steeghs, D., Karovska, M., et al. 2009, ApJ, 706, 738

APPENDIX

A. THE OPTICAL LIGHT CURVES

In this Appendix we present the optical light curves of our nova sample. These light curves are produced using V , g , CV (clear filter with V magnitude zero-point) or visual data from ASAS-SN and AAVSO. The time ranges were selected to highlight the timing of our spectroscopic observations around light curve peak.

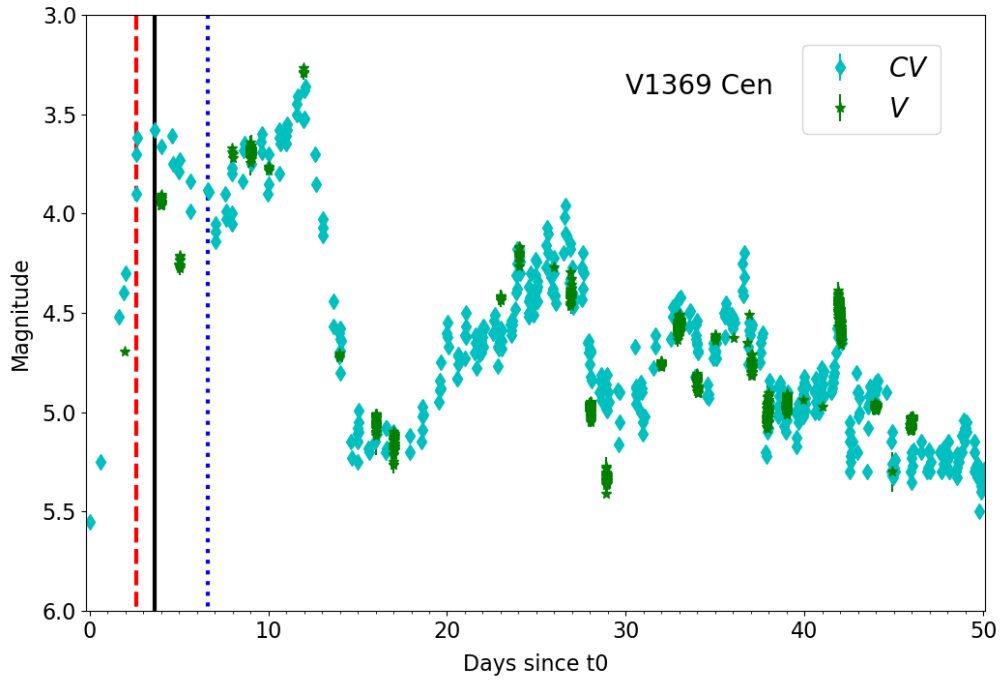


Figure A.1. The optical light curve of nova V1369 Cen color and symbol coded as indicated in the legend. The black solid line represents the date of the first optical peak (some novae exhibit multiple maxima). The red dashed line represents the date of the first optical spectrum and the blue dotted line represents the data of the second optical spectrum (see Table 1).

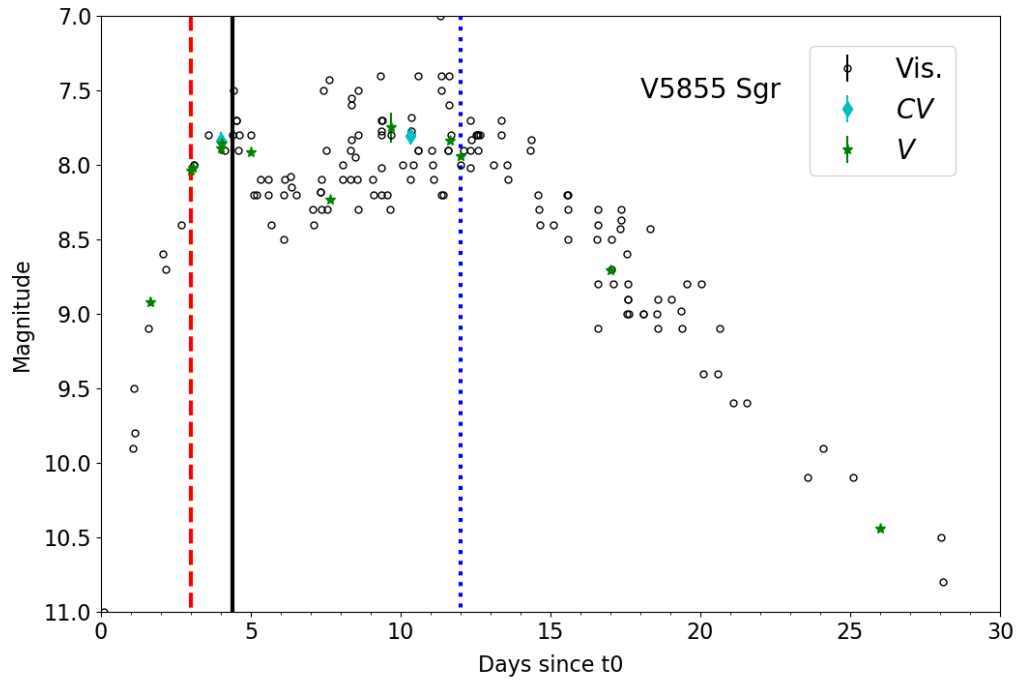


Figure A.2. Same as Figure A.1 but for nova V5855 Sgr.

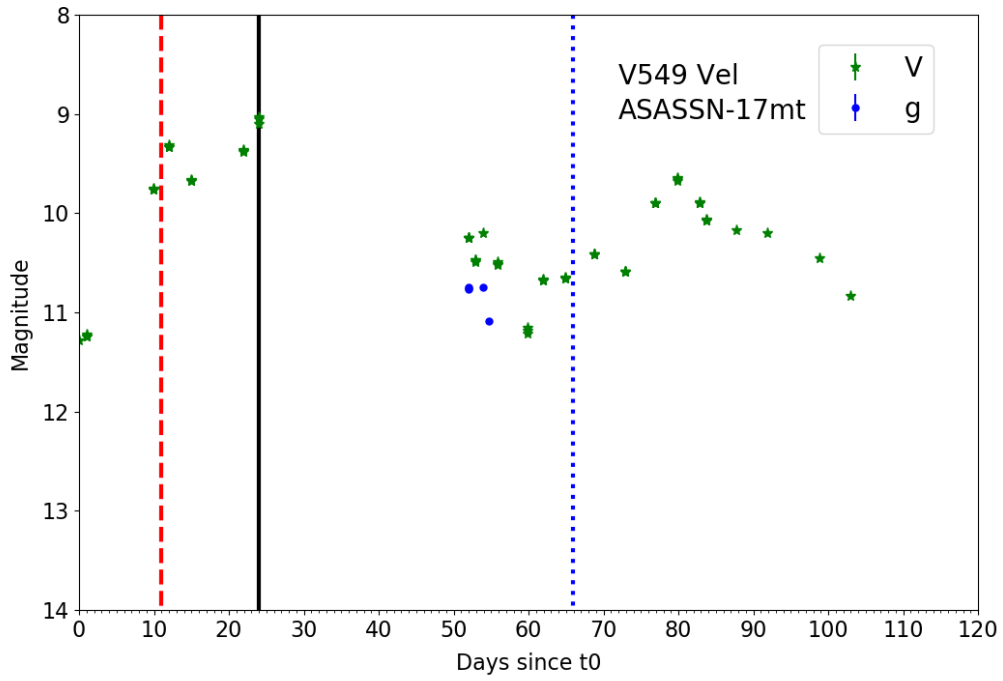


Figure A.3. Same as Figure A.1 but for nova V549 Vel (ASASSN-17mt).

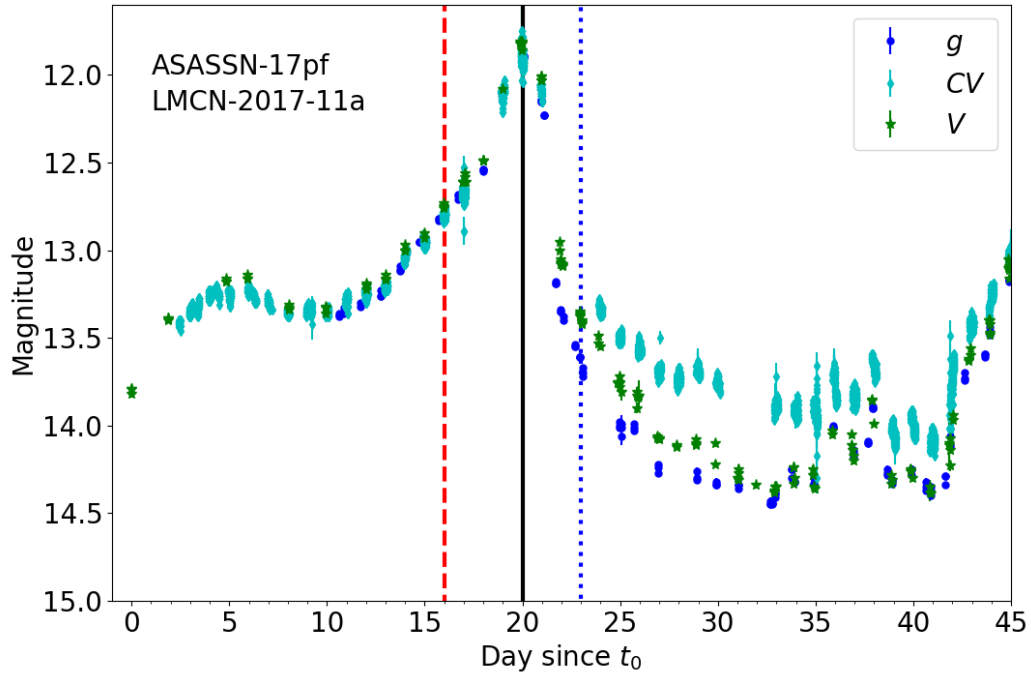


Figure A.4. Same as Figure A.1 but for nova LMCN-2017-11a (ASASSN-17pf).

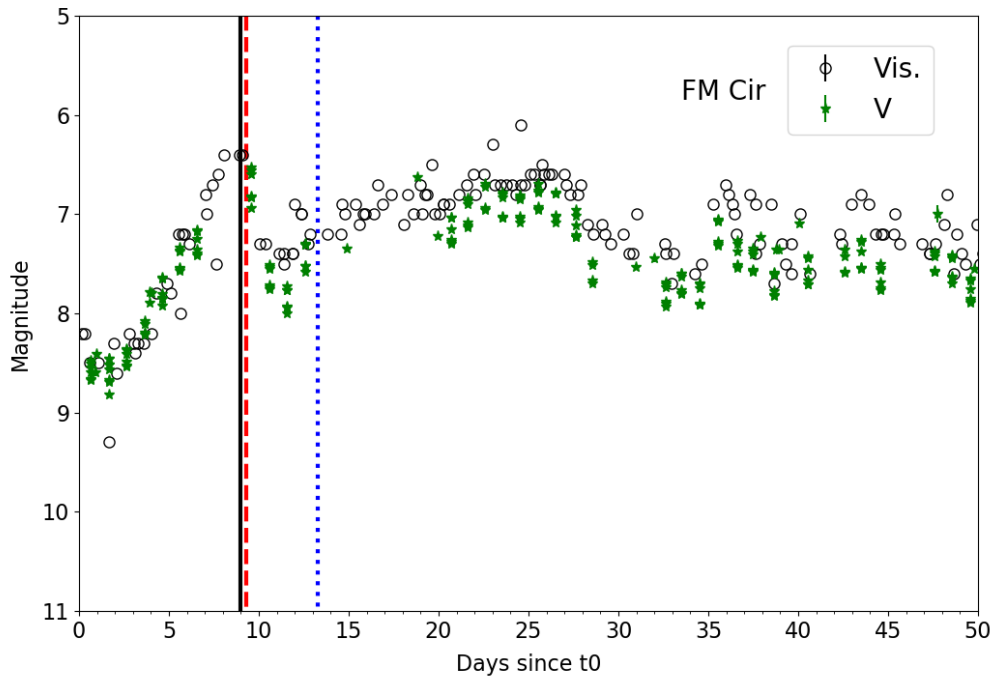


Figure A.5. Same as Figure A.1 but for nova FM Cir.

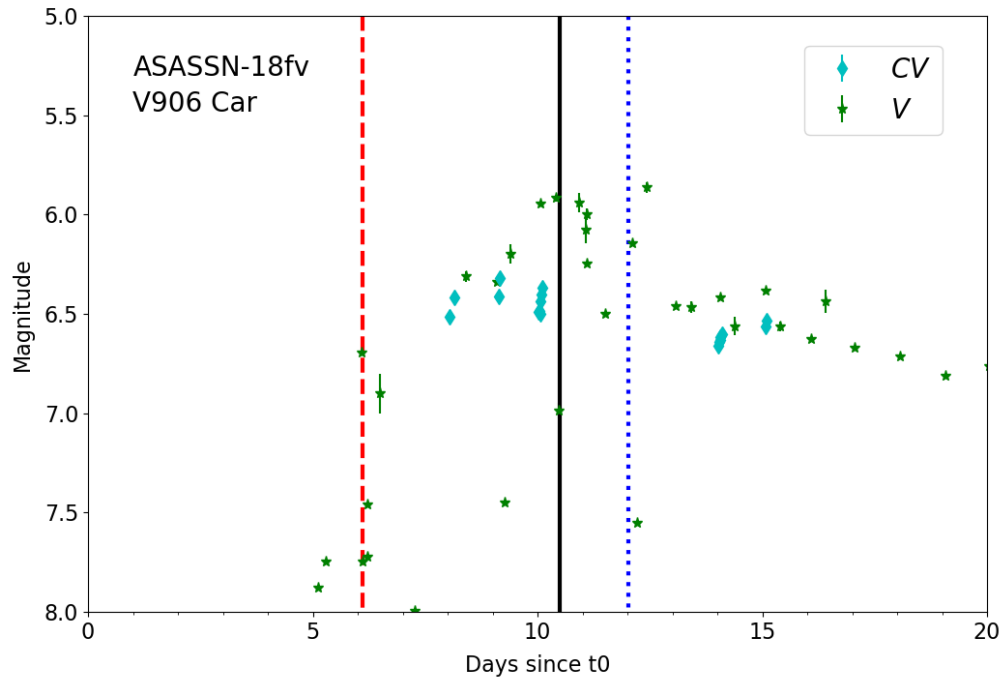


Figure A.6. Same as Figure A.1 but for nova V906 Car (ASASSN-18fv).

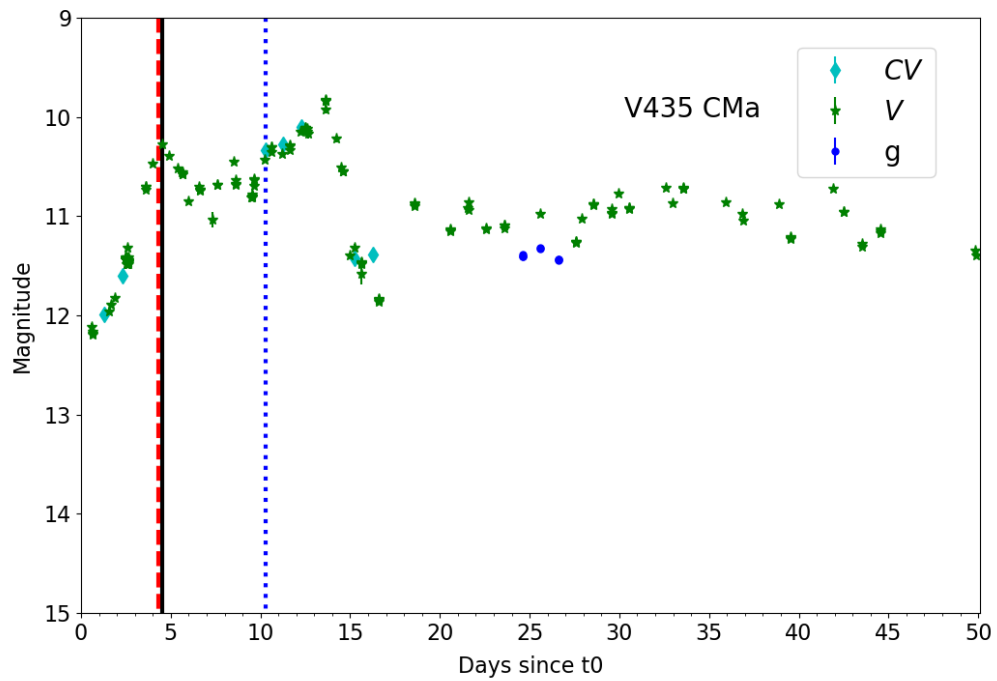


Figure A.7. Same as Figure A.1 but for nova V435 CMa.

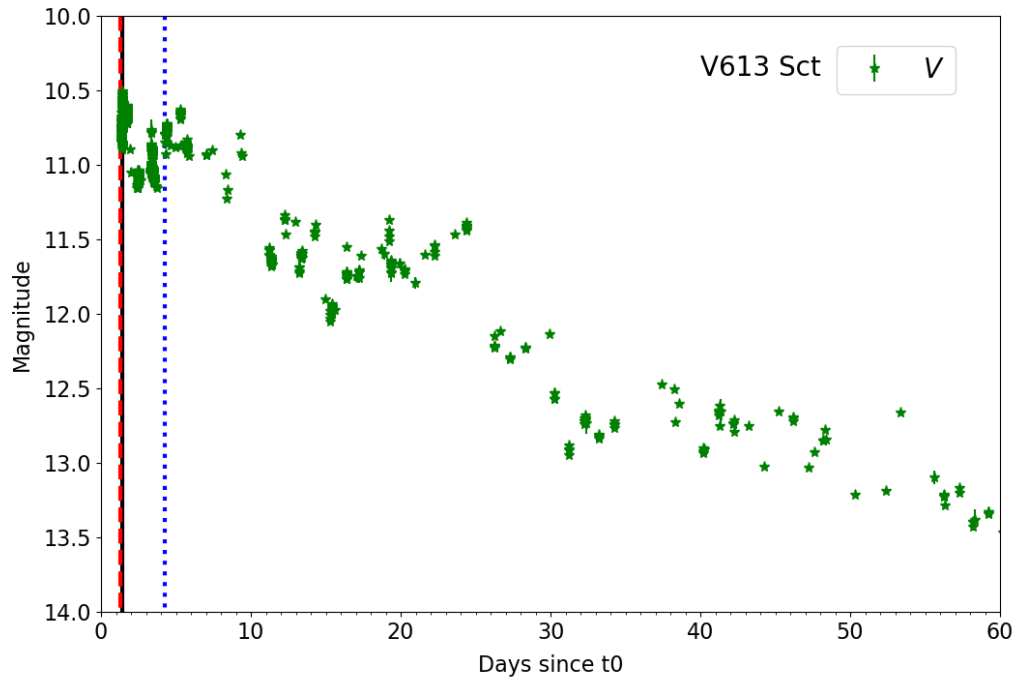


Figure A.8. Same as Figure A.1 but for nova V613 Sct.

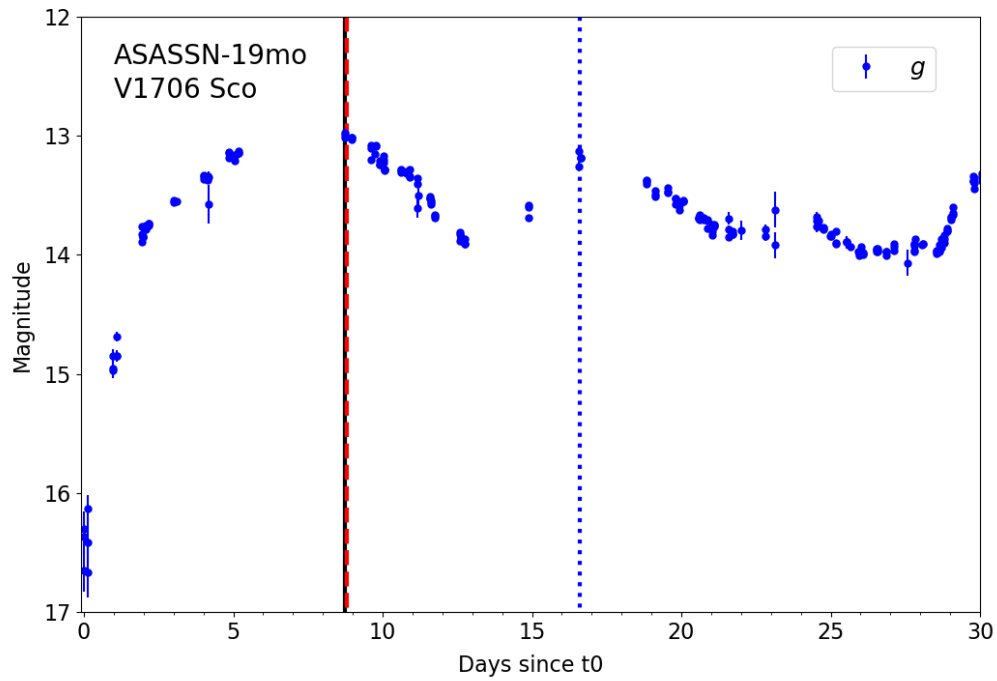


Figure A.9. Same as Figure A.1 but for nova V1706 Sco (ASASSN-19mo).

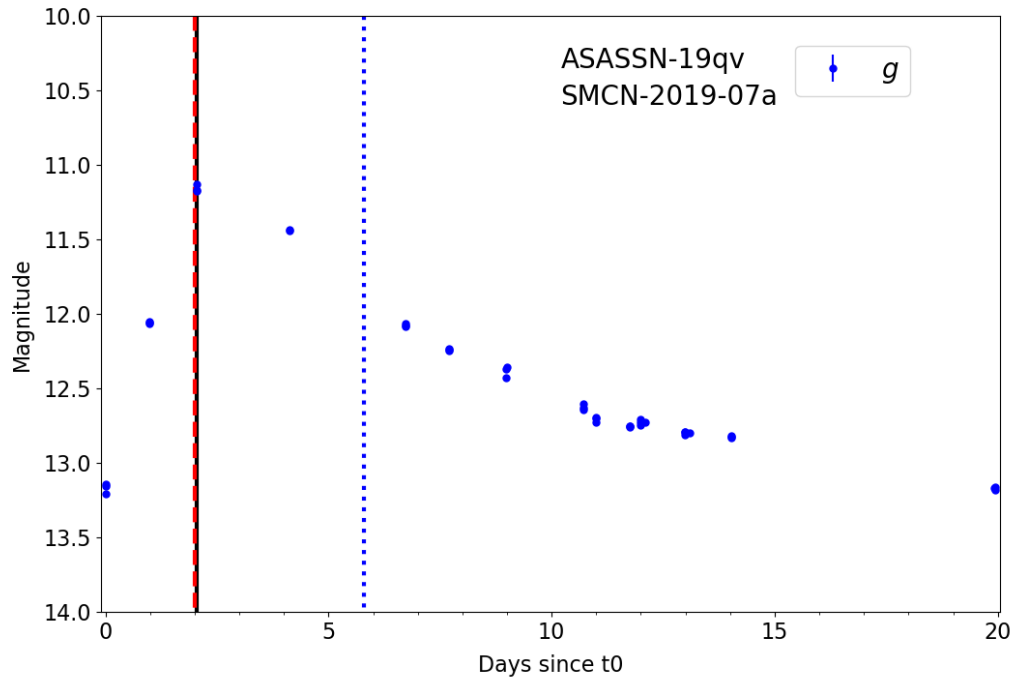


Figure A.10. Same as Figure A.1 but for nova SMCN-2019-07a (ASASSN-19qv).

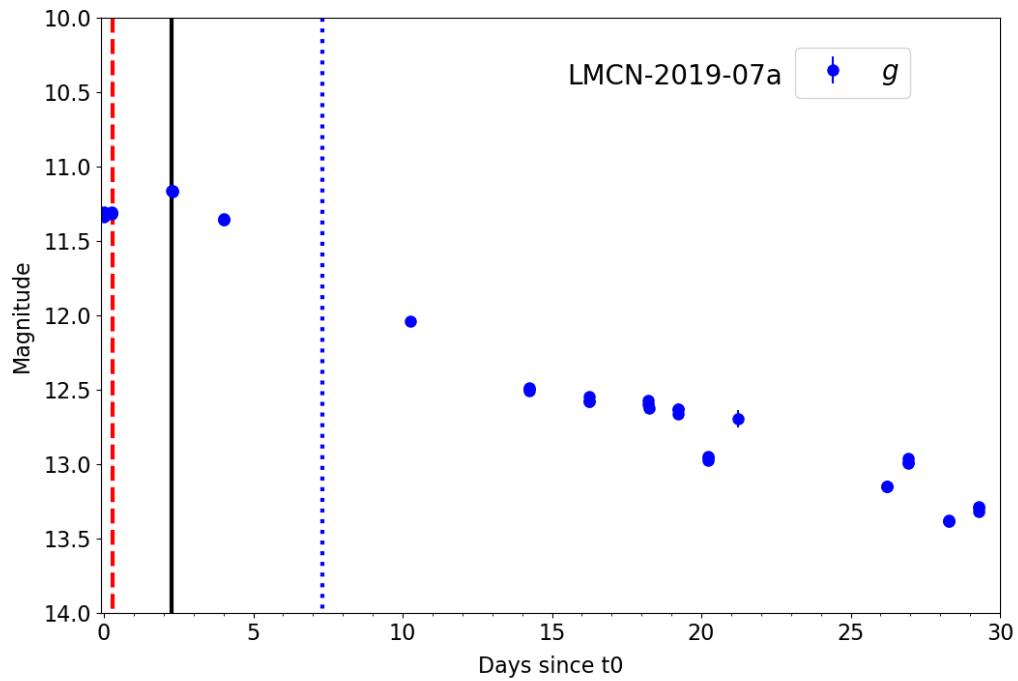


Figure A.11. Same as Figure A.1 but for nova LMCN-2019-07a.

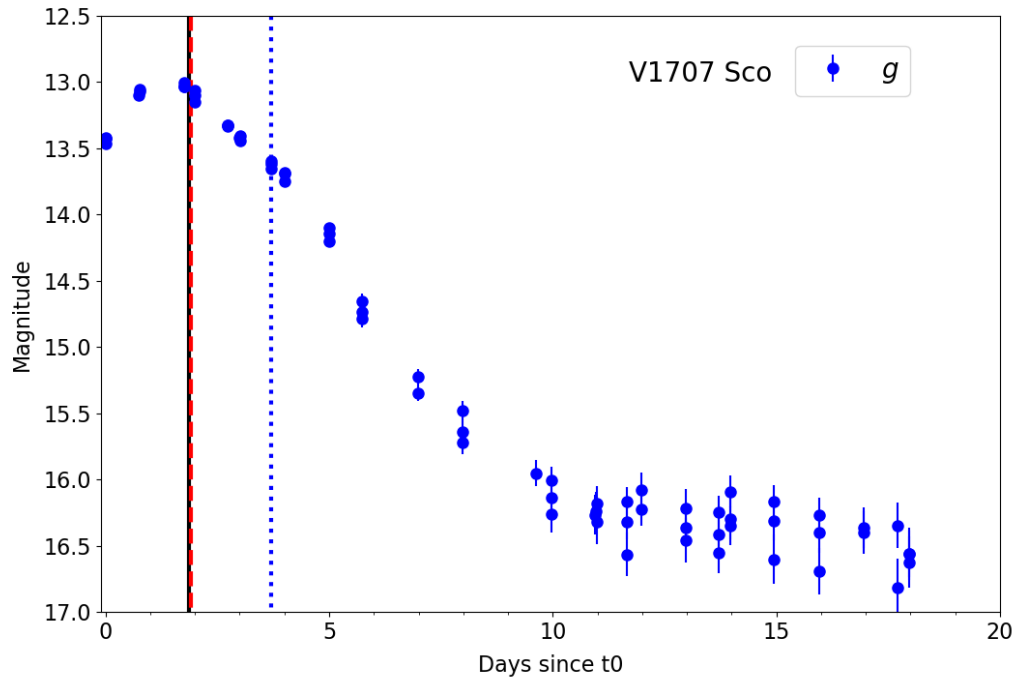


Figure A.12. Same as Figure A.1 but for nova V1707 Sco.

B. THE THEA LINE PROFILES

In this Appendix we present the THEA lines plot in comparison to the Na D, Fe II (42), and O I lines.

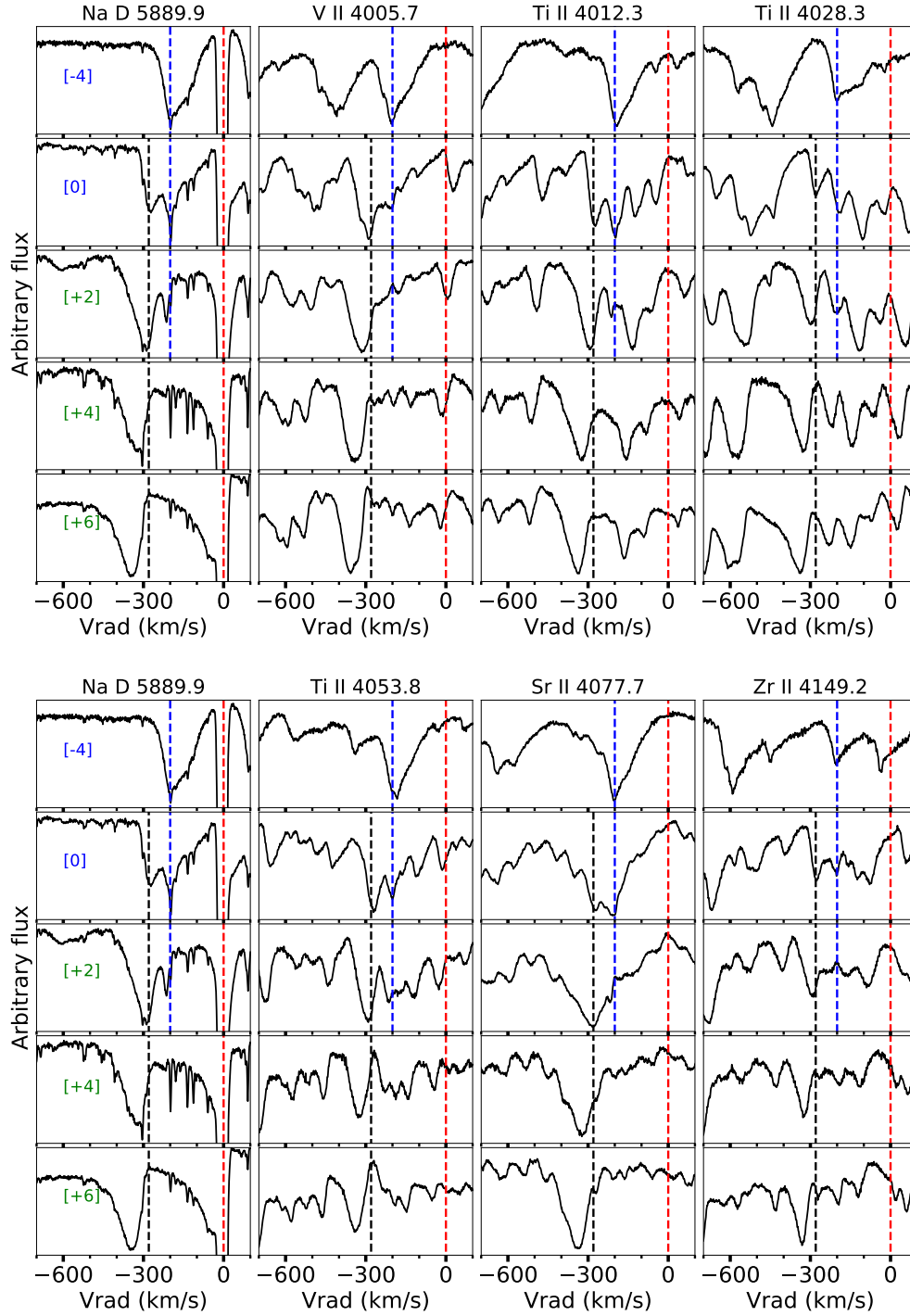


Figure B.1. Same as Figure 9 but for different THEA lines.

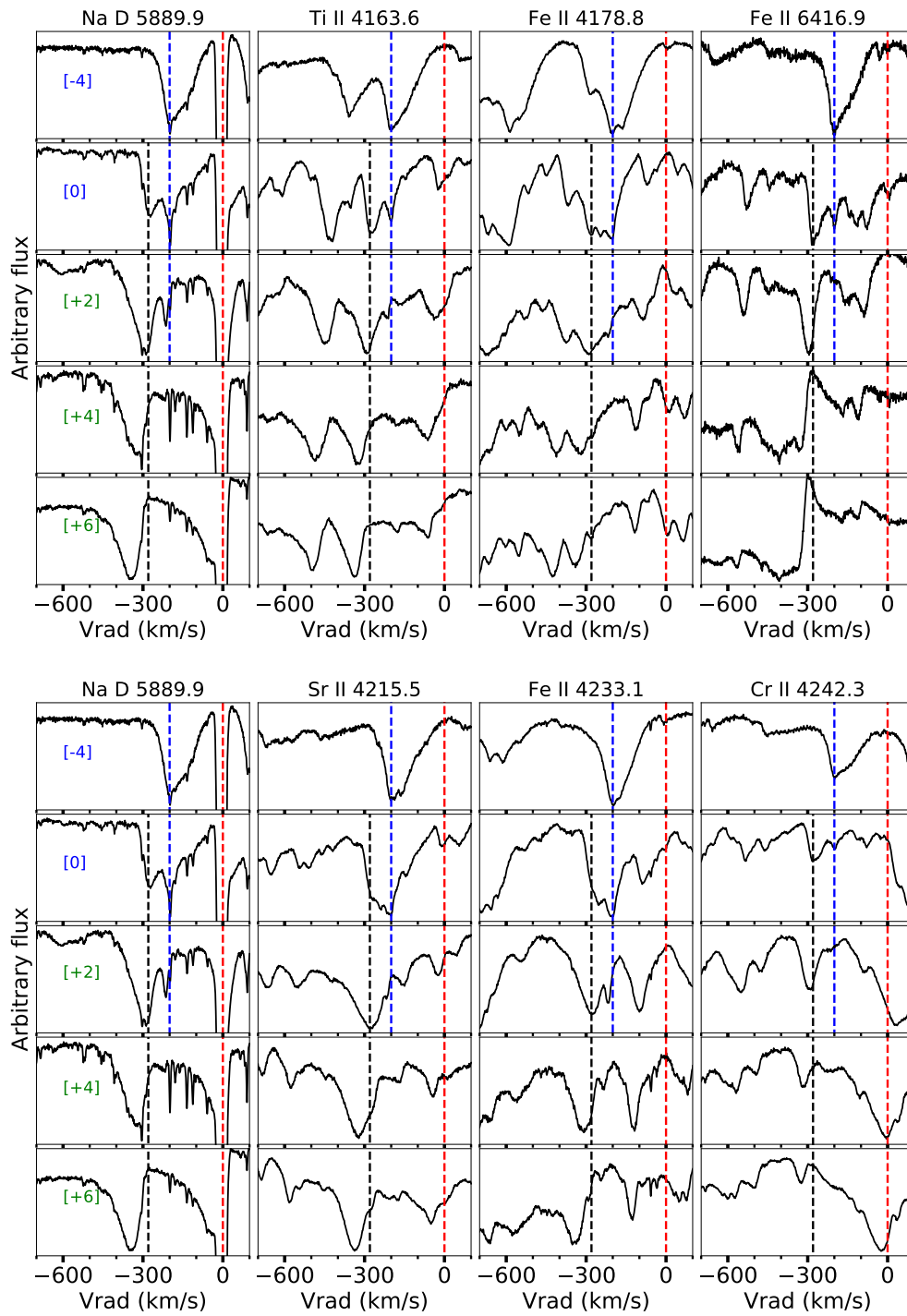


Figure B.2. Same as Figure 9 but for different THEA lines.

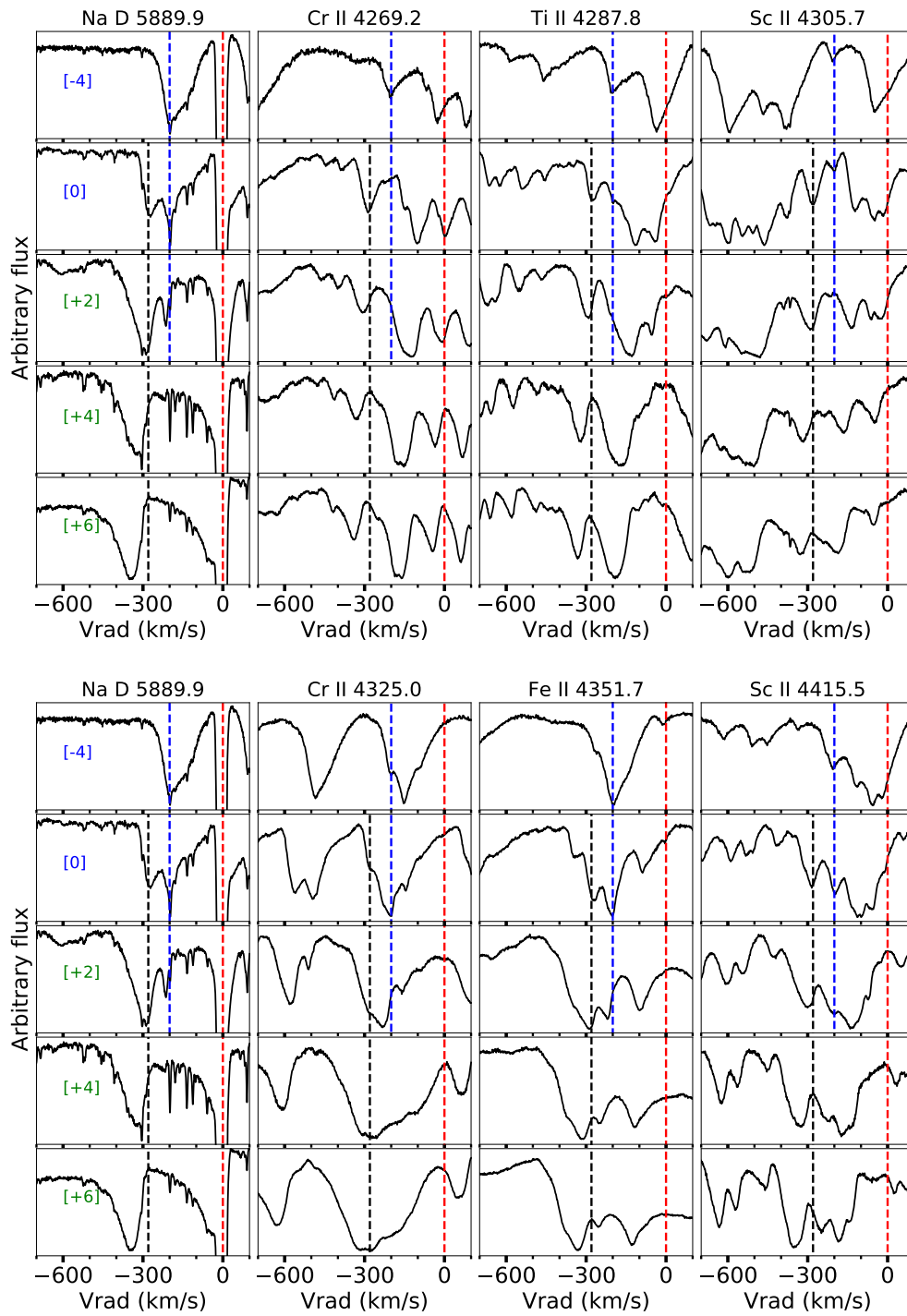


Figure B.3. Same as Figure 9 but for different THEA lines.

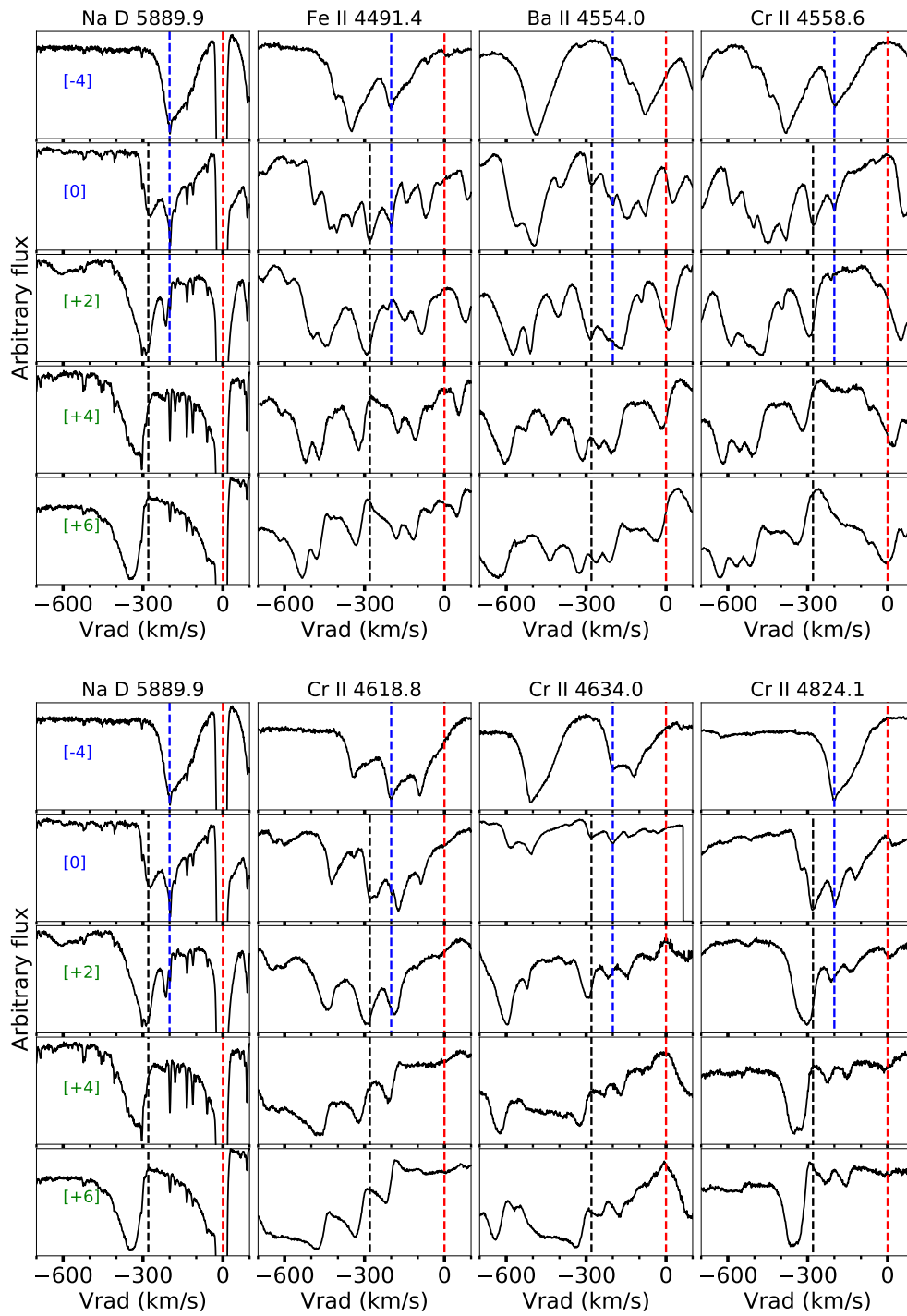


Figure B.4. Same as Figure 9 but for different THEA lines.

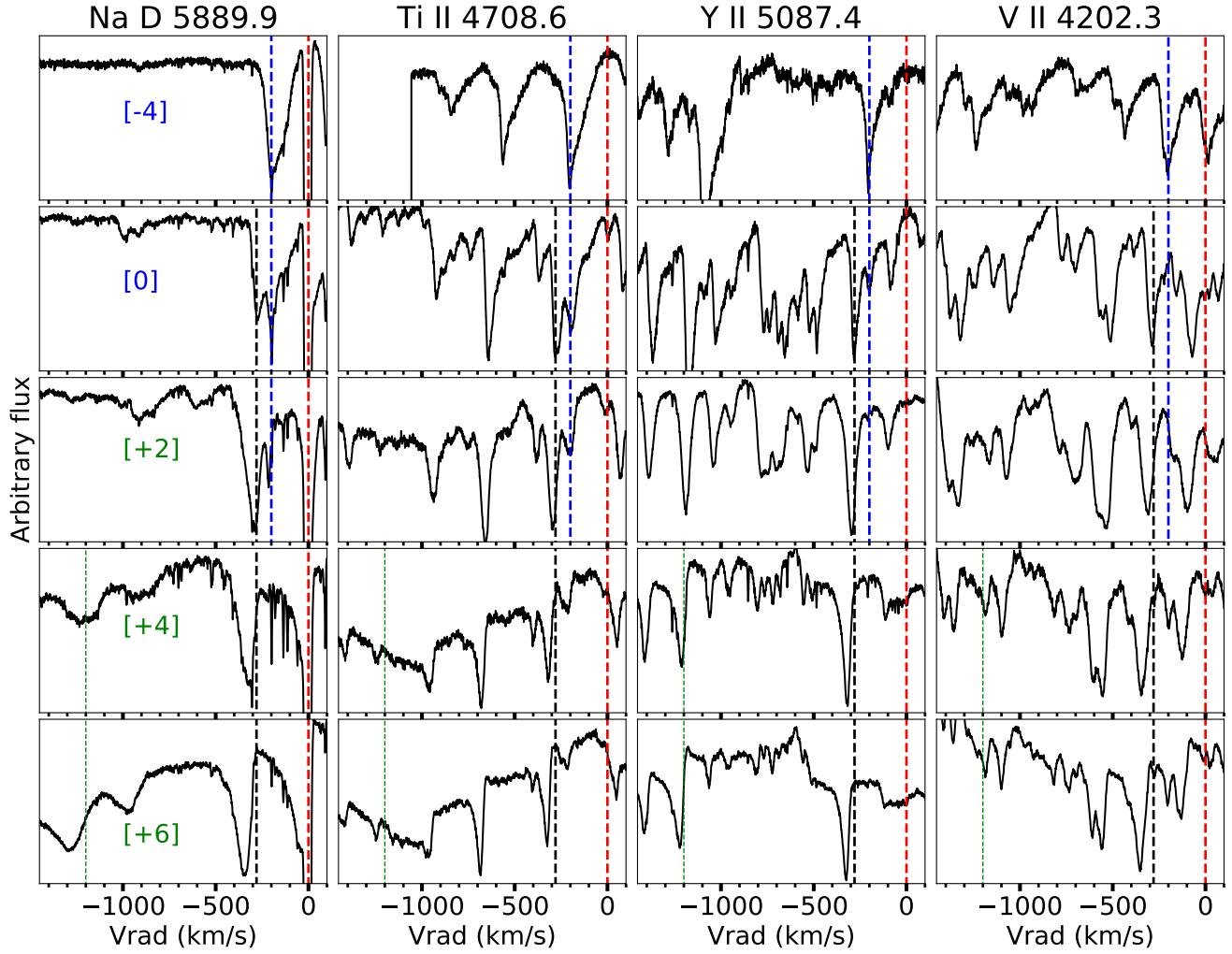


Figure B.5. The line profile evolution of a sample of THEA lines plotted in comparison to Na D at 5889.9 Å. The red vertical dashed line represents $v_{\text{rad}} = 0 \text{ km s}^{-1}$ (rest wavelength). The blue vertical dashed line marks a velocity of -200 km s^{-1} highlighting the slow component. The black dashed line marks a velocity of -300 km s^{-1} highlighting the intermediate component. The green dashed line marks a velocity of -1200 km s^{-1} highlighting the fast component, which can only be seen in the Na D line.

C. THE LINE PROFILE EVOLUTION OF SOME NOVAE

In this Appendix we present the evolution of the line profiles of $H\alpha$ for novae V435 CMa, V5855 Sgr, and V549 Vel.

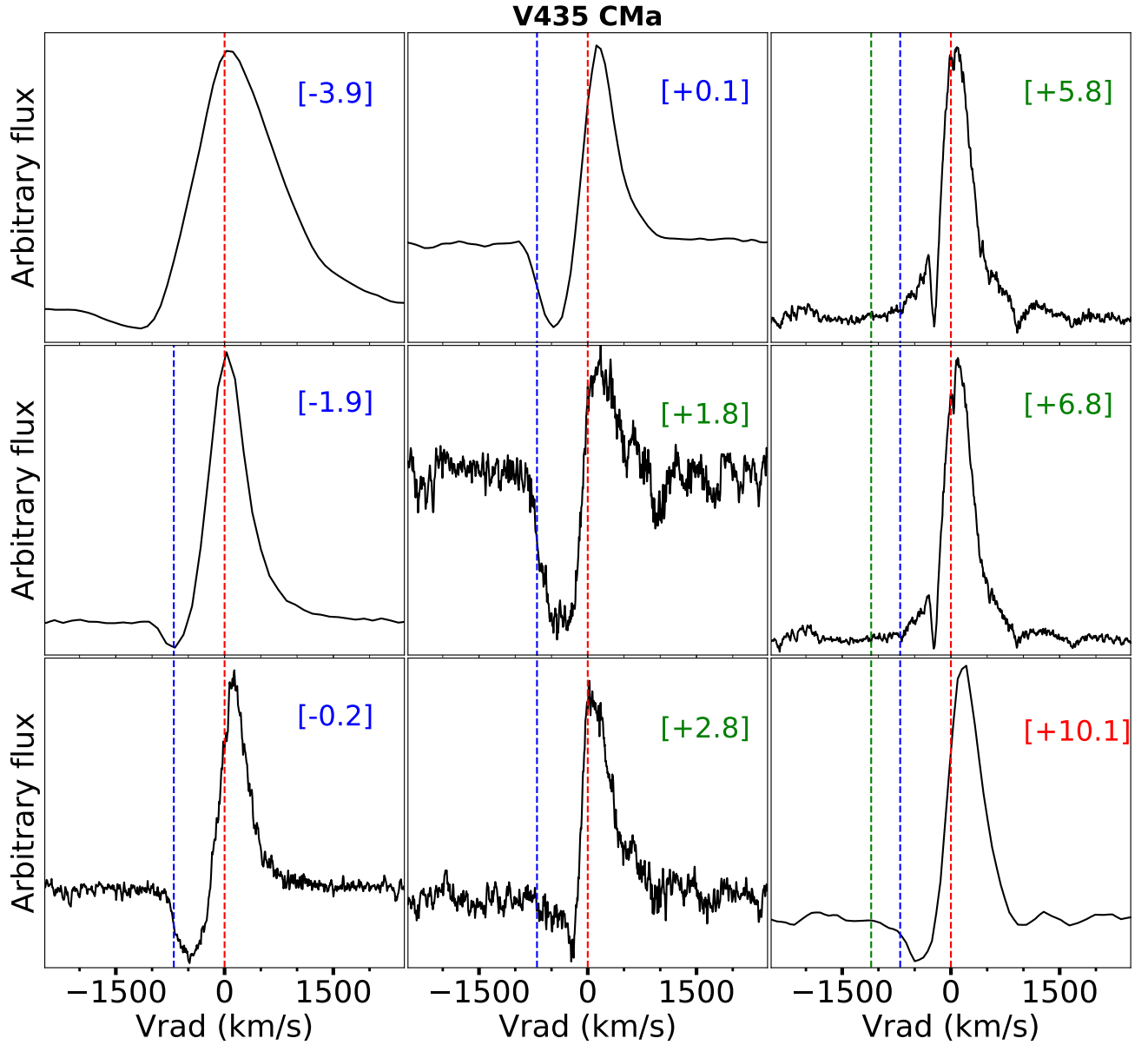


Figure C.1. The evolution of the $H\alpha$ line profiles for nova V435 CMa. The red, blue, and green dashed lines represent $v_r = 0 \text{ km s}^{-1}$ (estimate of the line center), -700 (the slow component), -1100 (the fast component), respectively. The numbers in brackets are days after discovery. The numbers in brackets are highlighted in blue and green are for observations taken before and after the first optical peak, respectively. The one highlighted in red is taken during the second optical peak. Heliocentric corrections are applied to all radial velocities.

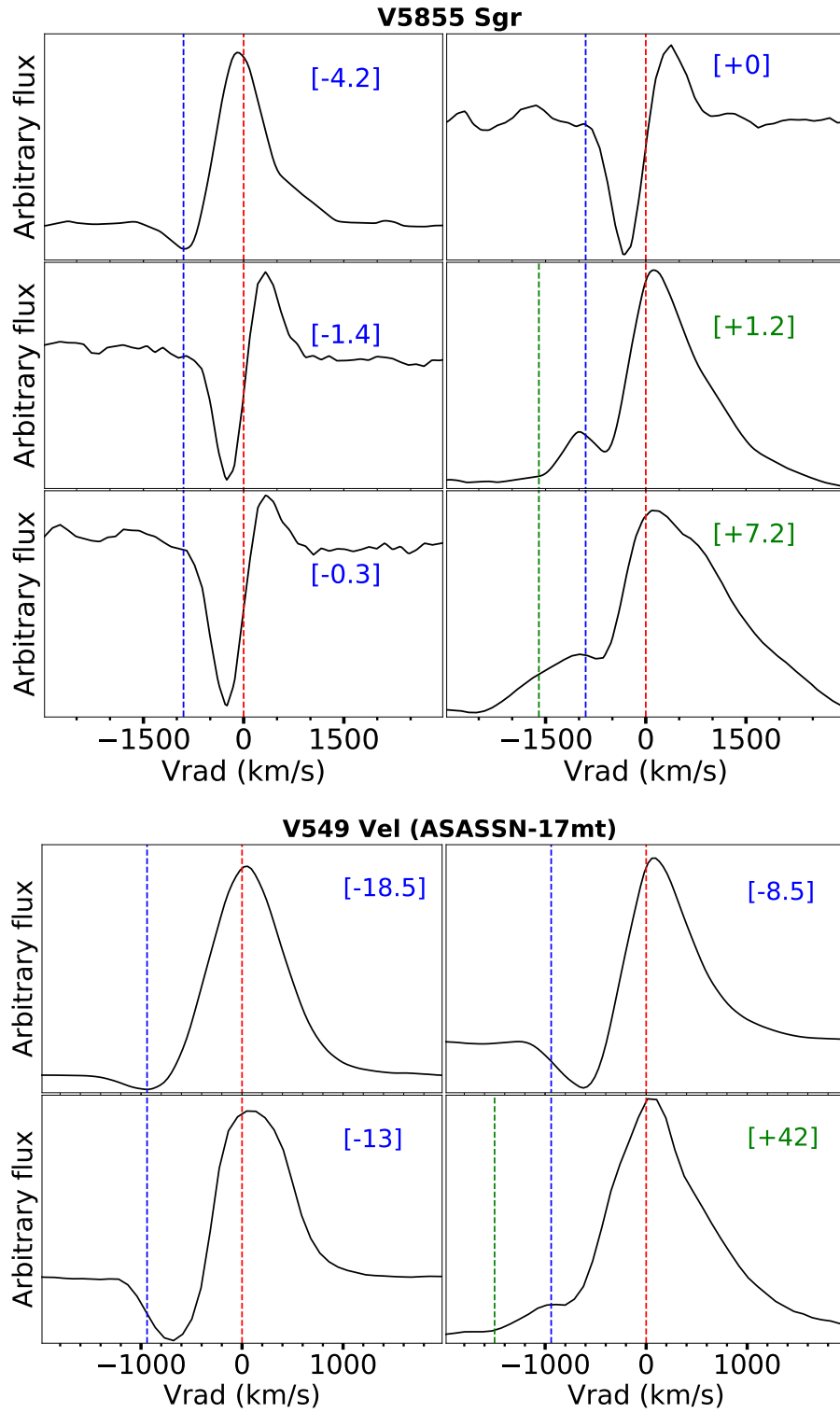


Figure C.2. The evolution of the $H\alpha$ line profiles for novae **V5855 Sgr** (*top*) and **V549 Vel** (*bottom*). In the top panel, the red, blue, and green dashed lines represent $v_r = 0 \text{ km s}^{-1}$ (rest wavelength), -900 km s^{-1} (the slow component), -1600 km s^{-1} (the fast component), respectively. In the bottom panel, the red, blue, and green dashed lines represent $v_r = 0$ (rest wavelength), -950 km s^{-1} (the slow component), -1500 km s^{-1} (the fast component), respectively. The numbers in brackets are days after discovery. The numbers in brackets are highlighted in blue and green are for observations taken before and after the optical peak, respectively. Heliocentric corrections are applied to all radial velocities.

Table D.4. Log of the spectroscopic observations of nova V906 Car adopted from Aydi et al. (2020).

$(t_s - t_{\max})$ (days)	Instrument	R	Range (Å)
-4	VLT-UVES	59,000	3050–9000
-2.5	VLT-UVES	59,000	3050–9000
-2	ARAS	11,000	6400–6720
-1	ARAS	11,000	6400–6720
-0.5	VLT-UVES	59,000	3050–9000
0	ARAS	11,000	6400–6720
+1	ARAS	11,000	6400–6720
+1.5	VLT-UVES	59,000	3050–9000
+2	ARAS	11,000	6400–6720
+4	VLT-UVES	59,000	3050–9000
+5	HERCULES	41,000	4000–10000
+6	ARAS	11,000	6400–6720
+7	HERCULES	41,000	4000–10000
+8	ARAS	11,000	6400–6720
+9	HERCULES	41,000	4000–10000
+10	HERCULES	41,000	4000–10000
+11.5	VLT-UVES	59,000	3050–9000
+13.5	VLT-UVES	59,000	3050–9000
+14	ARAS	11,000	6400–6720
+16	ARAS	11,000	6400–6720
+16.5	VLT-UVES	59,000	3050–9000
+20.5	SALT	67,000	3900–8800
+21.5	SALT	67,000	3900–8800
+24.5	VLT-UVES	59,000	3050–9000

Table D.5. Log of the CHIRON spectroscopic observations of nova FM Cir.

$(t_s - t_{\max})$ (days)	Instrument	R	Range (Å)
-7	CHIRON-SMARTS	27,000	4100–8900
-6	CHIRON-SMARTS	27,000	4100–8900
-5	CHIRON-SMARTS	78,000	4100–8900
-4	CHIRON-SMARTS	78,000	4100–8900
-2	CHIRON-SMARTS	78,000	4100–8900
-0.5	CHIRON-SMARTS	27,000	4100–8900

D. COMPLEMENTARY TABLES

In this Appendix we present complementary tables including log of observations for nova V906 Car and FM Cir.